Petroleum Science 20 (2023) 689–704

Contents lists available at ScienceDirect

Petroleum Science

journal homepage: www.keaipublishing.com/en/journals/petroleum-science

Original Paper

Wettability of different clay mineral surfaces in shale: Implications from molecular dynamics simulations

Kan-Yuan Shi [a, b], Jun-Qing Chen [a, c, d, *], Xiong-Qi Pang [a, b, **], Fu-Jie Jiang [a, b], Sha-Sha Hui [a, b], Zhen-Cheng Zhao [a, b], Di Chen [a, b], Qi Cong [d], Tong Wang [a, b], Hui-Yi Xiao [a, b], Xiao-Bin Yang [c, d], Yu-Ying Wang [c, d]

[a] State Key Laboratory of Petroleum Resources and Prospecting, China University of Petroleum, Beijing, 102249, China
[b] College of Geosciences, China University of Petroleum, Beijing, 102249, China
[c] Basic Research Center for Energy Interdisciplinary, College of Science, China University of Petroleum, Beijing, 102249, China
[d] Beijing Key Laboratory of Optical Detection Technology for Oil and Gas, College of Science, China University of Petroleum, Beijing, 102249, China

ARTICLE INFO

Article history:
Received 25 April 2022
Received in revised form
6 November 2022
Accepted 1 February 2023
Available online 8 February 2023

Edited by Jie Hao and Teng Zhu.

Keywords:
Shale
Molecular dynamics
Nanoscale
Wettability
Clay minerals

ABSTRACT

Shale contains a lot of clay minerals. Clay minerals mainly exist in nano- and micro-meter sized particles, and the pore structure is complex, which leads to its extremely complex wettability. The surface wettability of clay minerals significantly affects the oil and gas-bearing capacity of shale reservoirs. Therefore, studying the wettability of common clay minerals in shale at the nanoscale is of great significance for shale hydrocarbon exploration and development. In this study, the wetting behavior of water in *n*-hexane and toluene on different clay mineral surfaces at the nanoscale was systematically studied using Molecular dynamics (MD) simulation. And the influencing factors of wettability were analyzed. Through the analysis of the morphological changes of water, relative concentration of water, RDF and interaction energy, it is concluded that the following order of water wettability on the surfaces of clay minerals: montmorillonite > chlorite > kaolinite > illite. Through the analysis of interaction energy, it is concluded that the hydrophilicity of four clay minerals is stronger than that of lipophilicity. And the main interactions between water and oil and the mineral surfaces were van der Waals force and electrostatic force. In addition, the temperature, liquid hydrocarbon type, and mineralization of water affected the wettability of clay minerals. The concentration of water on the surfaces of montmorillonite, kaolinite, and illite decreased with increasing temperature, and the water wettability decreased. At 298 K, the hydrophilicity of the surfaces of the clay minerals in toluene follows the order montmorillonite > chlorite > kaolinite > illite. The higher the $NaHCO_3$ concentration in water, the weaker the wettability of the clay mineral surfaces to water. By comparing the previous experimental results with the MD simulation results, similar wetting characteristics were obtained, and the reliability of the simulation results was verified. MD simulation was used to explore the water wetting of the surfaces of four clay minerals in a shale reservoir from the micro level. This makes up for the lack of experimental means for clarifying the flow and production mechanisms of shale oil and gas and effectively improves the evaluation technology of shale.

© 2023 The Authors. Publishing services by Elsevier B.V. on behalf of KeAi Communications Co. Ltd. This is an open access article under the CC BY-NC-ND license (http://creativecommons.org/licenses/by-nc-nd/4.0/).

1. Introduction

In recent years, as important types of unconventional oil and gas, shale oil and gas account for an increasing proportion in the global energy structure and have become important alternative oil and gas resources (Law and Curtis, 2002; Jarvie, 2012; Jin et al., 2019; Hou et al., 2022; Hu et al., 2022a, 2022b). The estimated technically recoverable resources of shale oil in China's main basins amount to (3–6) × 10^9 t (Zou et al., 2019), showing a good development prospect. However, nanopore throat systems are widely developed in shale oil reservoirs. Although shale oil and gas have

* Corresponding author.
** Corresponding author.
E-mail addresses: chenjq@cup.edu.cn (J.-Q. Chen), pangxq@cup.edu.cn (X.-Q. Pang).

https://doi.org/10.1016/j.petsci.2023.02.001
1995-8226/© 2023 The Authors. Publishing services by Elsevier B.V. on behalf of KeAi Communications Co. Ltd. This is an open access article under the CC BY-NC-ND license (http://creativecommons.org/licenses/by-nc-nd/4.0/).

good reservoir capacities (Liu et al., 2020; Zhang et al., 2021), they also lead to huge viscous and molecular forces between fluids and surrounding media, resulting in retention (Li et al., 2020). Thus, these fluids generally cannot flow freely. Even if the temperature and pressure conditions are changed, they can only diffuse in the state of molecules or molecular clusters (Zou et al., 2012), which seriously affects shale oil and gas development. Therefore, studying the fluidity of shale oil and gas in nanopore throats is crucial.

Wettability is the key factor affecting the fluidity of shale oil. It usually refers to the diffusion or adhesion trend of a fluid in the presence of other immiscible fluids and significantly impacts on the accumulation process and the production behavior of oil and gas (Anderson and William, 1986; Morrow, 1990; Yoshimitsu et al., 2002; Alvarez and Schechter et al., 2016; Singh et al., 2022; Shi et al., 2022). The stronger the water wettability of minerals, the more conducive to the exploitation of oil and gas. Shale is mainly composed of clay minerals and brittle minerals (Boyer et al., 2006; Zhou et al., 2020; Li et al., 2021). The hydrophilicity of clay minerals is generally stronger than that of brittle minerals, and the influencing factors of their wettability are complex (Li et al., 2020). The wettability of organic matter and different mineral components in rocks varies greatly. The wettability of organic matter is related to the type, maturity and elemental composition of organic matter. There are also great differences in the wettability of different mineral components. Even the same mineral will have different wettabilities due to different mineral structure, surface properties and environment (Li, 2021). The mineral composition of rocks in shale is an important factor affecting wettability (Barclay and Worden, 2000). Different mineral surfaces have different adsorption effects on polar compounds, so they may have different wettability characteristics (Xi et al., 2019). Under normal formation water conditions, the surface of carbonate minerals is more prone to oil wetting than that of silicate minerals (Chilingar and Yen, 1983). In silicate minerals, the surface of quartz is preferentially combined with the hydrogen bond of water molecules, showing water wetting; Feldspar may show mixed wetting characteristics (Stumm, 1992; Ehrenberg et al., 1995). Clay minerals usually exhibit different wettabilities due to differences in chemical composition, morphology and physical structure (Boneau and Clampitt, 1977). For example, kaolinite with small and dispersed crystals tends to be wetted by water, while kaolinite with large crystals may be wetted by oil (Al-Shafei and Okasha, 2009). Illite usually appears as water wetting (Schmatz et al., 2015). Silicate and carbonate minerals rich in iron, such as montmorillonite, chlorite, and iron dolomite, may be prone to oil wetting (Wang and Guidry, 1994). Fassi-Fihri et al. (1995) found that expansive clay is more lipophilic than non-expansive clay. In the process of burial, montmorillonite must undergo long-term diagenetic evolution, and the diagenetic reaction in the reservoir may lead to the change of wettability (Maurice, 1967). Since the surface of solid components may be covered with minerals such as tar pitch, iron oxide, trace montmorillonite, chlorite and trace carbonate, some hydrophilic minerals may become hydrophobic (Lan et al., 2014). Therefore, studying the wettability of clay minerals in shale reservoirs is of great significance to the exploration, resource evaluation, and development mode of shale oil resources (Gao and Hu, 2018; Yassin et al., 2017).

In recent years, the wettability has been measured using various technologies. These include the Amott wettability index (Amott, 1958), USBM wettability index (Donaldson et al., 1969), contact angle measurement (Lu et al., 2003; Edward, 2018; Li et al., 2021), spontaneous imbibition method (Morrow, 1990), Atomic force microscopy (Pan et al., 2020; Zhang et al., 2022), micro-computed tomography (μCT) imaging method (Scanziani et al., 2017; Arif et al., 2020; Guo et al., 2022), and nuclear magnetic resonance (NMR) T_2 method (Al-Garadi et al., 2022). However, the measurement of clay mineral contact angles is affected by many factors, including surface roughness, temperature, surface heterogeneity, swelling, and the existence of ions (Scanziani et al., 2017; Arif et al., 2020; Al-Garadi et al., 2022). Thus, previous studies obtained very different results using different experimental techniques (Shang et al., 2010; Yin et al., 2012; Pan et al., 2020). At present, wetting angle method is a common method to measure wetting angle (Pan et al., 2020). However, under actual geological conditions, the wettability is related to the complexity and heterogeneity of mineral composition (Omidi et al., 2017). The wettability measured on a single plane under the experimental conditions will be different from that under the actual underground conditions (Pan et al., 2020). Therefore, in order to truly measure the wetting angle of underground conditions, the temperature and pressure similar to the underground conditions should be set. This is very difficult and expensive for macroscopic experimental measurement. Therefore, finding a feasible method for studying the inherent wettability of different clay minerals in shale on the nanoscale has guiding significance for shale oil exploitation (Salehi et al., 2008; Xue et al., 2015). MD is a method used in the computer simulation of matter at the atomic or molecular level. It has been developing for a long time, and its application range continues to widen (Hu et al., 2016; Pham et al., 2021). MD simulation has been developed to study the inherent wettability of nanosolid surfaces. For instance, Zhang et al. (2016) studied the interactions between clay minerals and closed pore fluid using MD simulation. They revealed the effects of surface groups, layer charges, and salts on the wettability. Chang et al. (2018) systematically studied the wetting of nanoscale water on different rock surfaces. Yi et al. (2018) calculated the adsorption energy between a montmorillonite surface and water molecules using MD simulation. They qualitatively characterized the wettability of the montmorillonite surface affected by surface charge and ions. Mohammed and Gadikota (2020) studied the self-assembly and related wettability changes of asphaltene on illite at 20 MPa and 313 K by using classical MD simulation. Chen et al. (2020) studied the wettability of modified clay using the MD simulation. Their results were similar to those obtained using the solid drop method, verifying the accuracy of this method. Therefore, molecular dynamics simulation is a powerful tool for studying nanoscale wettability. At present, for MD methods, the previous work mainly focuses on mineral–H_2O–CO_2/CH_4 or mineral–H_2O–air, and there are few manuscripts specially studying the wettability of clay minerals using MD (Pan et al., 2019, 2020; Al-Yaseri et al., 2022; Hou et al., 2022). Therefore, the clay mineral–H_2O–liquid hydrocarbon we studied is very necessary.

The above contents show a lack of systematic research on the surface wettability of clay minerals in shale, especially in micro measurement research. In this paper, the inherent wettability of clay minerals in shale was systematically studied on the nanoscale using MD simulation. First, based on MD simulation, the water wettability of four common clay minerals (montmorillonite, kaolinite, chlorite, and illite) in different liquid hydrocarbons (*n*-hexane and toluene) was simulated, and the effects of temperature, pressure and salinity on the wettability were analyzed. Then, by comparing MD simulation results with the previous experimental results, similar wetting characteristics were obtained, and the reliability of the simulation results was verified. The research methods and results of this paper made up for the lack of experimental means, and provide important practical significance for clarifying the flow and production mechanisms of shale oil and gas.

2. Models and methods

2.1. Molecular model

MD was used to simulate the wettability of different clay mineral surfaces. First, the "water–liquid hydrocarbon–clay mineral" model was established. In this model, kaolinite ($Al_4[Si_4O_{10}](OH)_8$) was derived from the database of the Materials Studio, and montmorillonite ($K_2[Si_4O_8]_6[Al_{10}Mg_2O_{12}(OH)_{12}]$) (Heinz et al., 2005), chlorite ($Mg_{12}[Si_8O_{20}](OH)_{16}$) (Lister and Bailey, 1967), and illite ($K_4[Al_8Si_4O_{20}](OH)_4$) (Gualtieri, 2000) were derived from the American Mineralogist Crystal Structure Database. We have uploaded the Materials Studio files of montmorillonite, kaolinite, chlorite, and illite as supplementary materials. Montmorillonite is a 2:1 structured clay mineral with an O layer sandwiched between two T layers (Yi et al., 2016; Zhao et al., 2017; Pan et al., 2020). Isomorphous substitutions often occur in these layers, e.g. Al^{3+} substitution by Mg^{2+} in the O layer and Si^{4+} substitution by Al^{3+} in the T layer. Illite is a class of trilayer silicates with varying degrees of lattice substitution (Si^{4+} is substituted by Al^{3+} in the T layer). Therefore, cations are often attracted to the mineral surface to compensate for the negative surface charge (Zheng and Zaoui, 2017; Pan et al., 2020). Shale oil is mainly composed of saturated hydrocarbons, aromatic hydrocarbons, non-hydrocarbons and asphaltenes, of which saturated hydrocarbons account for about 30%–70% and aromatic hydrocarbons account for about 25%–60% (Xiong et al., 1965; Lu and Xue, 2021). In this study, *n*-hexane was chosen to represent saturated hydrocarbon and toluene was chosen to replace aromatic hydrocarbon. The most common montmorillonite, kaolinite, chlorite, and illite minerals in the clay minerals (El-Shater et al., 2021; Li et al., 2021) were used for the simulation. The specific cell structure and cell parameters are shown in Fig. 1 and Table 1.

In establishing the model, we first established an oil box (60 Å × 60 Å × 40 Å) filled with liquid hydrocarbons (Fig. 2a) and then a water box containing 300 water molecules (20.8 Å × 20.8 Å × 20.8 Å) (Fig. 2b) and a clay mineral with a horizontal surface (Fig. 2c). The basis for selecting the number of water molecules is to try to choose according to one-third of the size of the oil box and mineral surface, because if there are too many water molecules, the water molecules will not spread on the mineral surface, and if the water molecules are too small, it will affect the observation of water wettability. Then, the rock surface was fixed and the periodic boundary conditions were applied in the X, Y, and Z directions. Second, the shale oil box, water box, and clay mineral structure were respectively optimized. Finally, the optimized oil box, water box, and clay minerals were combined into one using the Materials Studio software to obtain the wettability model (Fig. 2d), and the combined wettability model was optimized. A vacuum layer with a thickness of 40 Å was added to the *Z*-axis to prevent the periodic influence of this axis.

Table 1
Unit cell parameters of clay minerals.

Parameters	Montmorillonite	Kaolinite	Chlorite	Illite
a/Å	5.192	5.149	5.336	5.223
b/Å	13.523	8.934	9.240	9.018
c/Å	20.046	7.384	14.370	20.143
α/°	90.000	91.930	90.000	90.000
β/°	95.735	105.042	96.930	95.665
γ/°	90.000	89.791	90.000	90.000

a, b, and c are the lengths of the unit cell. a, β, γ are the angles of the unit cell.

2.2. Simulation force field and parameters

The accuracy of molecular simulation results depends on the reasonable setting of force field and simulation parameters (Chang et al., 2018; Heydari et al., 2021). The setting of force field and simulation parameters needs to match the actual geological conditions. In this study, COMPASS force field is selected for simulation. The COMPASS force field is the first high-quality force field integrating organic and inorganic material parameters (Tavakoli and Tarighat, 2016). It can deal with organic and inorganic molecular systems, effectively solve covalent bond model, ion model, quasi ion model and metal model, and simulate various small and large molecules, including organic molecules, gaseous molecules and inorganic molecules. The COMPASS force field, which has been used in many molecular simulations involving mineral surfaces, was selected to study the interaction between atoms (Sun, 1998; Chang et al., 2018). In recent years, it has been used by most people to study the interface simulation of clay minerals and organic matter. Wei et al. (2009) used the COMPASS force field to simulate the movement of cetyltrimethylammonium bromide in montmorillonite. Babatunde et al. (2021) used the COMPASS force field to simulate the adsorption of CO_2 and CH_4 on the surface of montmorillonite and illite. Zhang et al. (2021) simulated the adsorption of xanthate and polyacrylamide on kaolinite surface under compass force field. The following are the settings of various simulation parameters. The Andersen thermostat method was used to keep

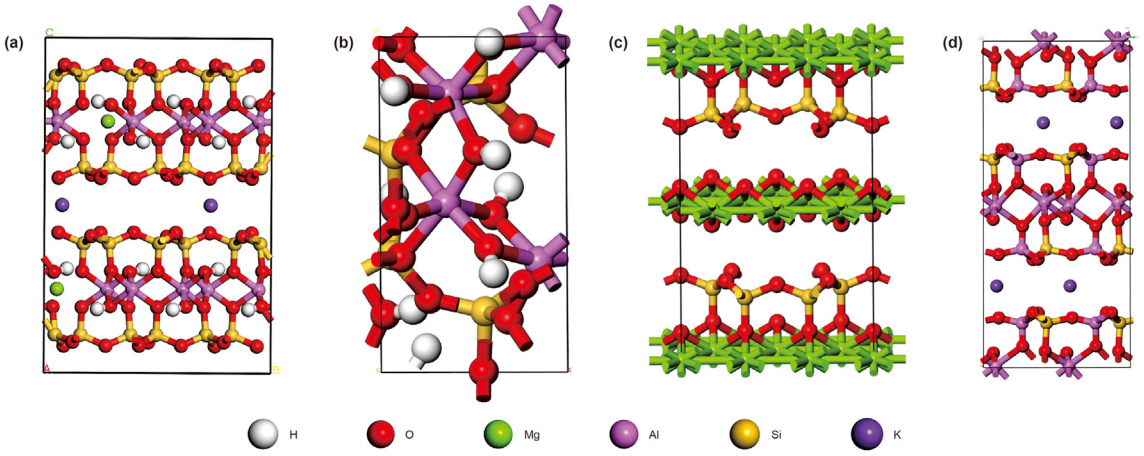


Fig. 1. Crystal structure of the clay minerals. (a) montmorillonite; (b) kaolinite; (c) chlorite; (d) illite.

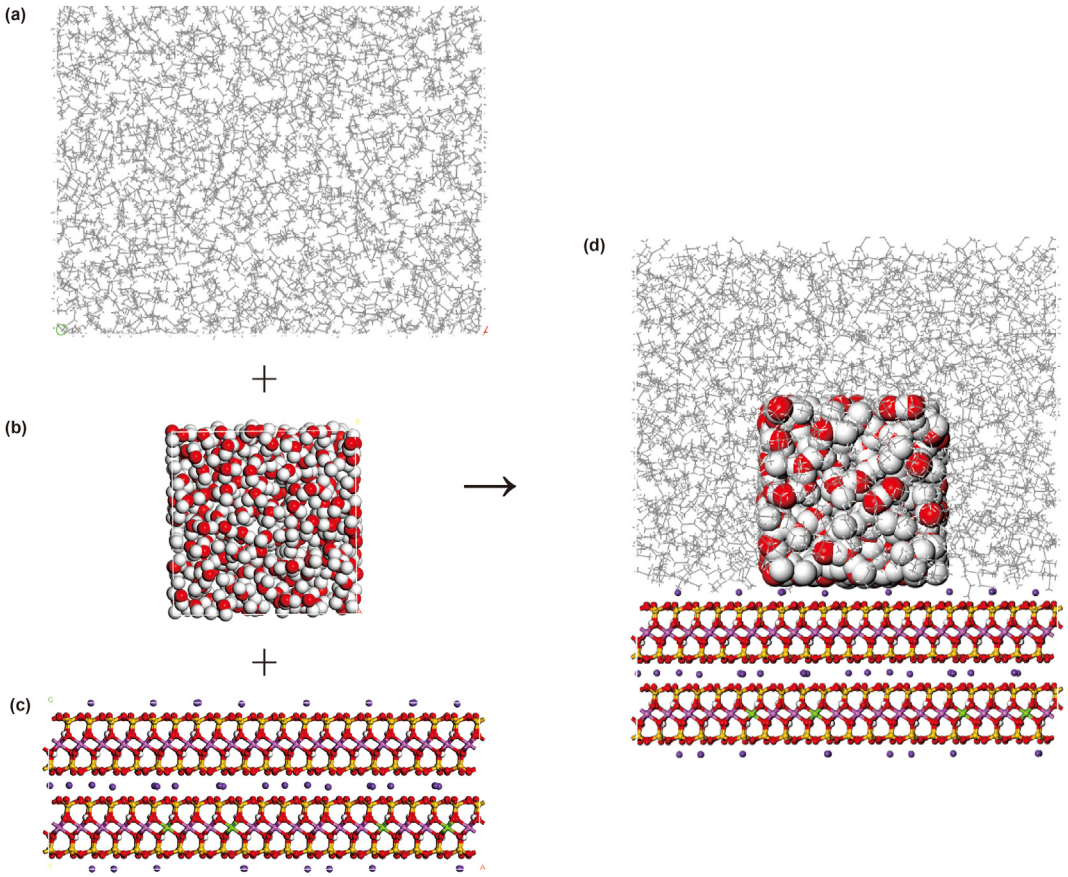


Fig. 2. Establishment process of the wettability model. (a) Shale oil; (b) water; (c) montmorillonite minerals; (d) initial model of the oil–water wettability of montmorillonite minerals.

the temperature unchanged (Andersen, 1980), the high-precision Ewald method was used to calculate the electrostatic interaction (Zhong et al., 2013), and the steepest center methods optimized the structure of the initial model (Chang et al., 2018). The cut-off distance was set as 12.5 Å is set to improve the calculation efficiency (Xia et al., 2016). The main input parameters in the balancing process during the simulation are shown in Table 2. All simulations were repeated with 1 fs (Zhu et al., 2015). The system was simulated at 1000 ps under the canonical ensemble (NVT), which ensured the accuracy of the simulation.

2.3. Measurement of contact angle in MD

In this paper, geometric methods are used to extract key physical quantities to calculate the contact angle (Fan and Cagin, 1995; Li and Wang, 2017; Dong et al., 2021; Shi et al., 2022). When the mineral interface is hydrophilic, the contact angle between the corresponding droplet and the interface is an acute angle (Fig. 3a), whereas the hydrophobic surface exhibits an obtuse angle (Fig. 3b). The contact angle can be derived from the following geometric equations:

Table 2
Main parameters in the simulation process.

Simulation Modules	Parameter	Input	Unit
Amorphous Cell-Packing	Density of water box	1.000	g/cm^3
	Density of *n*-hexane box	0.660	g/cm^3
	Loading steps	1000	/
Geometry Optimization	Maximum number of iterations	500	/
	Algorithm	Steepest descent	/
Dynamics-NVT	Density of the whole system (montmorillonite)	0.787	g/cm^3
	Density of the whole system (kaolinite)	0.567	g/cm^3
	Density of the whole system (chlorite)	0.729	g/cm^3
	Density of the whole system (illite)	0.820	g/cm^3
	Time step	1	fs
	Total simulation time	1000	ps
	Number of steps	1000000	/
	Thermostat	Andersen	/
	Initial velocities	Random	/

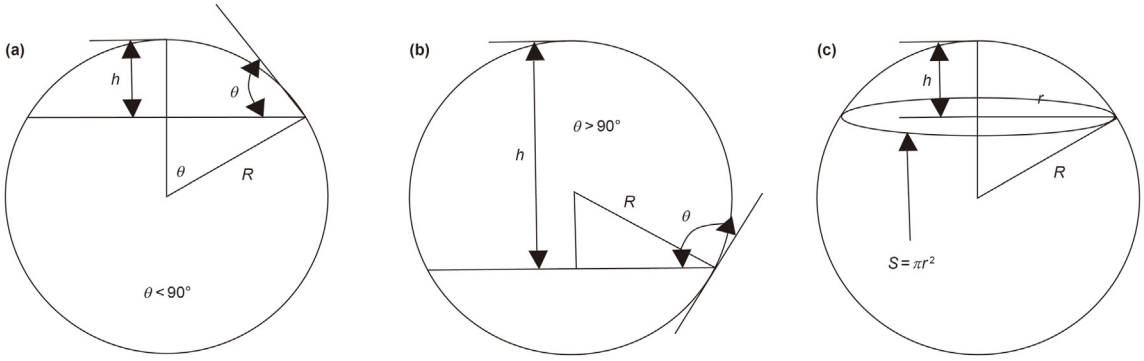


Fig. 3. The contact angle is (a) acute angle, (b) obtuse angle, (c) three-dimensional view.

$$\cos\theta = 1 - h/R \tag{1}$$

$$(R-h)^2 + r^2 = R^2 \tag{2}$$

$$S = \pi r^2 \tag{3}$$

Based on above-mentioned equations, the contact angle is described by:

$$\theta = \arccos\frac{S - \pi h^2}{S + \pi h^2} \tag{4}$$

where h represents the height from the center of the liquid circle to the surface of the solid mineral; R represents the radius of the sphere corresponding to the droplet; θ is the contact angle; S denotes droplet bottom area.

The value of S is obtained by the lattice method. The water-mineral interface is divided into 1 Å × 1 Å lattice and S is the sum of all the lattices, h is obtained by measuring the height from the center point of the water droplet to the mineral surface. After obtaining the meshed differential model of the water droplets, the contact angle of the water droplets on the mineral surface can be obtained based on Eq. (4).

3. Results

The wettability of water in *n*-hexane and toluene on different clay mineral surfaces (montmorillonite, kaolinite, chlorite, and illite) was simulated using molecular dynamics. Under NVT, the temperature was set to 298 K, and MD simulation at 1000 ps was conducted for eight "oil–water–clay mineral" wettability models. Model screenshots at different simulation times (100, 250, 600, 800, and 1000 ps) were taken to analyze and compare the change process of the water droplets. The oil–water concentration on the surface of clay minerals, radial distribution function (RDF) and interaction energy, and the wettability characteristics of each mineral were obtained and finally compared with the experimental results. When calculating the relative concentration and distance parameters, first click the Forcite module in the MS software, and then select the concentration profile in the Analysis to obtain the relative concentration curve. After that, the distance between water or liquid hydrocarbon and the mineral surface can be obtained by subtracting the thickness of the mineral from the abscissa value of the relative concentration curve.

3.1. Study on the wettability of clay minerals in n-hexane

This simulation adopted the montmorillonite structure, where the charge is balanced by potassium ions between layers. With increasing simulation time, water droplets were rapidly adsorbed to the montmorillonite surface. When the simulation reached about 100 ps, the water droplets were completely tiled on the surface of montmorillonite, and the water molecules exhibited directional arrangement characteristics (Fig. 4a). When studying the difference between hydrogen bond and van der Waals force, Steiner and Desiraju (1998) proposed that when the adsorption distance is less than 3 Å, the bonding type between adsorbent and adsorbate is hydrogen bond, and vice versa is van der Waals force. The main forms of judging the existence of hydrogen bond are energy method and geometric judgment method. In this paper, the geometric judgment method is used to judge the hydrogen bond, that is, hydrogen bond occurs when the adsorption distance is less than 3 Å. It can be seen from Fig. 5a that water molecules are close to the mineral surface, indicating that in the process of montmorillonite adsorbing water molecules, oxygen in water molecules and hydrogen atoms on the surface of kaolinite form hydrogen bonds. This leads to the directional arrangement of water molecules on the surface of montmorillonite. The water molecules were adsorbed in about four layers on the surface of montmorillonite. Oil molecules were also adsorbed in obvious layers. The first water layer was close to the montmorillonite surface and had a higher concentration than that of the first oil layer (Fig. 5a), indicating that the hydrophilicity of the montmorillonite surface was stronger than that of oil. We found that the negatively charged montmorillonite surface had a strong electrostatic attraction for exchangeable cations. These exchangeable cations had very strong hydration capacities, which endowed the clay minerals with their overall hydrophilicity (Yi et al., 2018).

Kaolinite is a kind of dioctahedral clay mineral, which is formed by 1:1 arrangement of silica tetrahedron and alumina octahedron. Water molecules will not be attached between layers. Therefore, the adsorbed water of kaolinite only exists on the surface of kaolinite crystal. In order to determine the hydrophilic surface and hydrophobic surface of kaolinite, Solc et al. (2011) analyzed the diffusion behavior of water droplets on different surfaces of kaolinite by means of molecular dynamics simulation. The results show that the contact angle of water droplets on O surface (alumina octahedral surface) is 0°, while the contact angle on T surface (silica tetrahedral surface) is 105°, indicating that O surface is hydrophilic surface and T surface is hydrophobic surface (Pan et al., 2020).

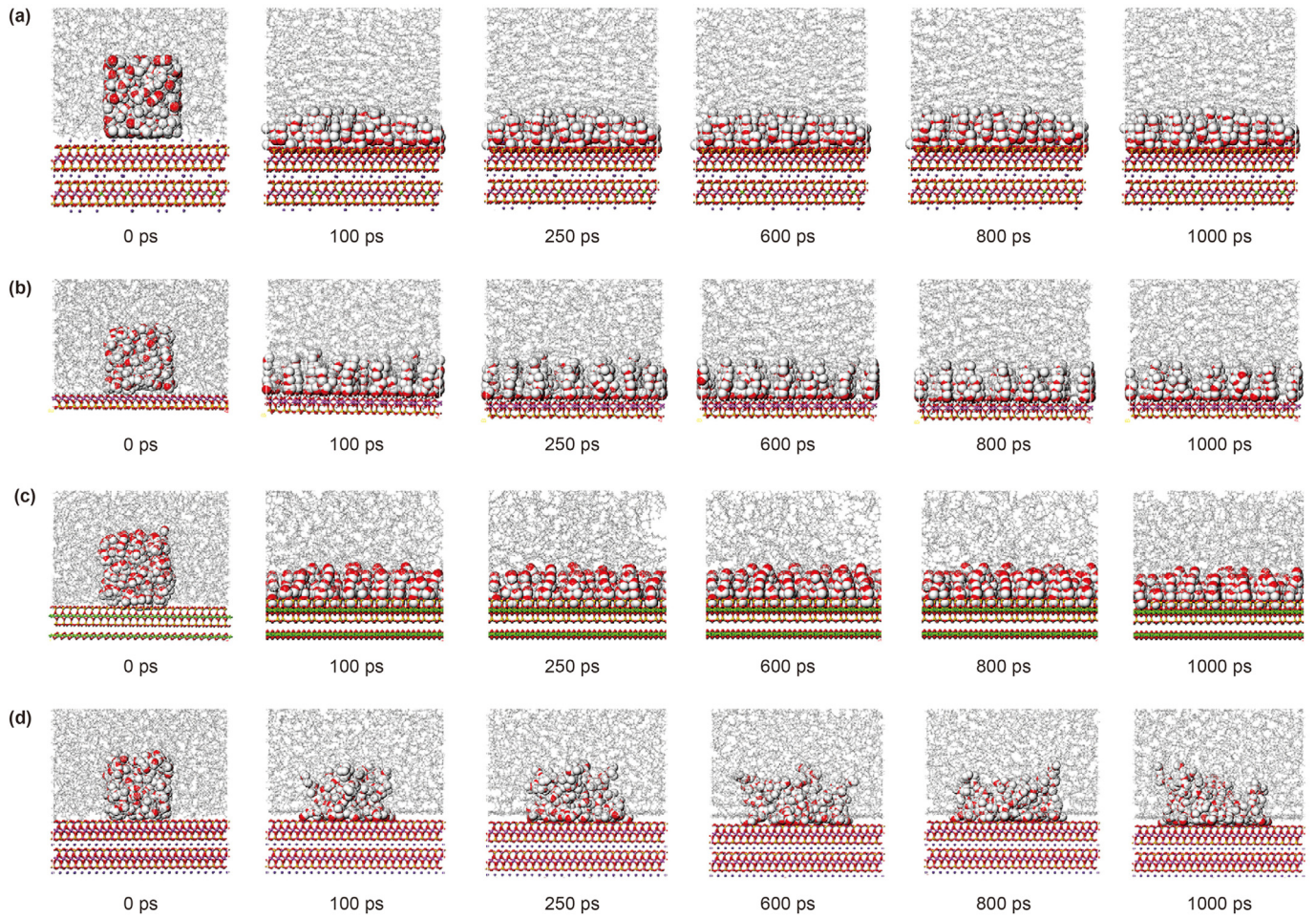


Fig. 4. Simulation screenshot of the oil–water wettability of clay minerals in *n*-hexane. (a) montmorillonite; (b) kaolinite; (c) chlorite; (d) illite.

Therefore, in this study, the 001 surface of kaolinite is cut to make the O surface of kaolinite directly contact with water and oil, regardless of the influence of T surface. With increasing simulation time, water droplets were adsorbed to one side of the kaolinite surface, and a directional rehearsal of the water molecules occurred. The reason for the directional arrangement is that the oxygen atoms of the water molecules faced the hydrogen atoms on the kaolinite surface (Fig. 4b), and the −OH groups on the kaolinite surface tended to form multiple stable hydrogen bonds with the water molecules. About five adsorption layers were observed on the surface of kaolinite. Layered adsorption of oil molecules was also noted. The first adsorption layer of water was close to the first adsorption layer of oil from the kaolinite surface (Fig. 5b). Therefore, we considered that the kaolinite surface had strong water and oil wettability, which could be explained by the existence of surface hydroxyl groups. It could provide a large number of hydrogen bond sites and promote the formation of strong hydrogen bonds (Du and Miller, 2007). This is consistent with the result obtained by Luo et al. (2019) using a self-priming experiment, where kaolinite is hydrophilic.

With increasing simulation time, water droplets were adsorbed on the chlorite surface. When the simulation reached 100 ps, the water droplets were completely tiled on the chlorite surface (Fig. 4c). Moreover, a directional arrangement of the water molecules was occurred on the chlorite surface because the hydrogen atoms of the water molecules form hydrogen bonds with the oxygen atoms on the mineral surface, so that the hydrogen atoms in the water molecules gradually adsorb to the mineral surface. From the oil and water concentration distribution of the chlorite wettability system, we can see that the chlorite surface was completely covered with water molecules, whereas the oil molecules were not distributed at the place closest to the chlorite surface (Fig. 5c). It is considered that the water wettability of the chlorite surface is much stronger than its oil wettability, consistent with previous research results (Zhang et al., 2020).

For the wettability model of illite, with increasing simulation time, water droplets were gradually adsorbed to the mineral surface. The shape of the water droplets gradually changed from square to oblate sphere and presented a certain angle with the mineral surface. Although there are oxygen atoms on the surface of illite minerals, and the hydrogen atoms in water molecules can form hydrogen bonds with the oxygen atoms on the mineral surface, in illite, because the cohesion energy of water molecules (9237.03336 kcal/mol, Eq. (5)) is stronger than the interaction force between water molecules and mineral surface (2089.46767 kcal/mol, see the section of 3.3 for detailed calculation), the water molecules can not be fully spread on the mineral surface and can not be aligned on the illite surface (Wu, 2018). The cohesion energy of a liquid can be used to measure its intermolecular cohesion. The greater the cohesion energy, the stronger the intermolecular cohesion, and the less prone to deformation. When the simulation reached 800 ps, the angle between the water droplets and the mineral surface hardly changed (Fig. 4). Using the geometric method (Fan and Cagin, 1995; Li and Wang, 2017; Dong et al., 2021),

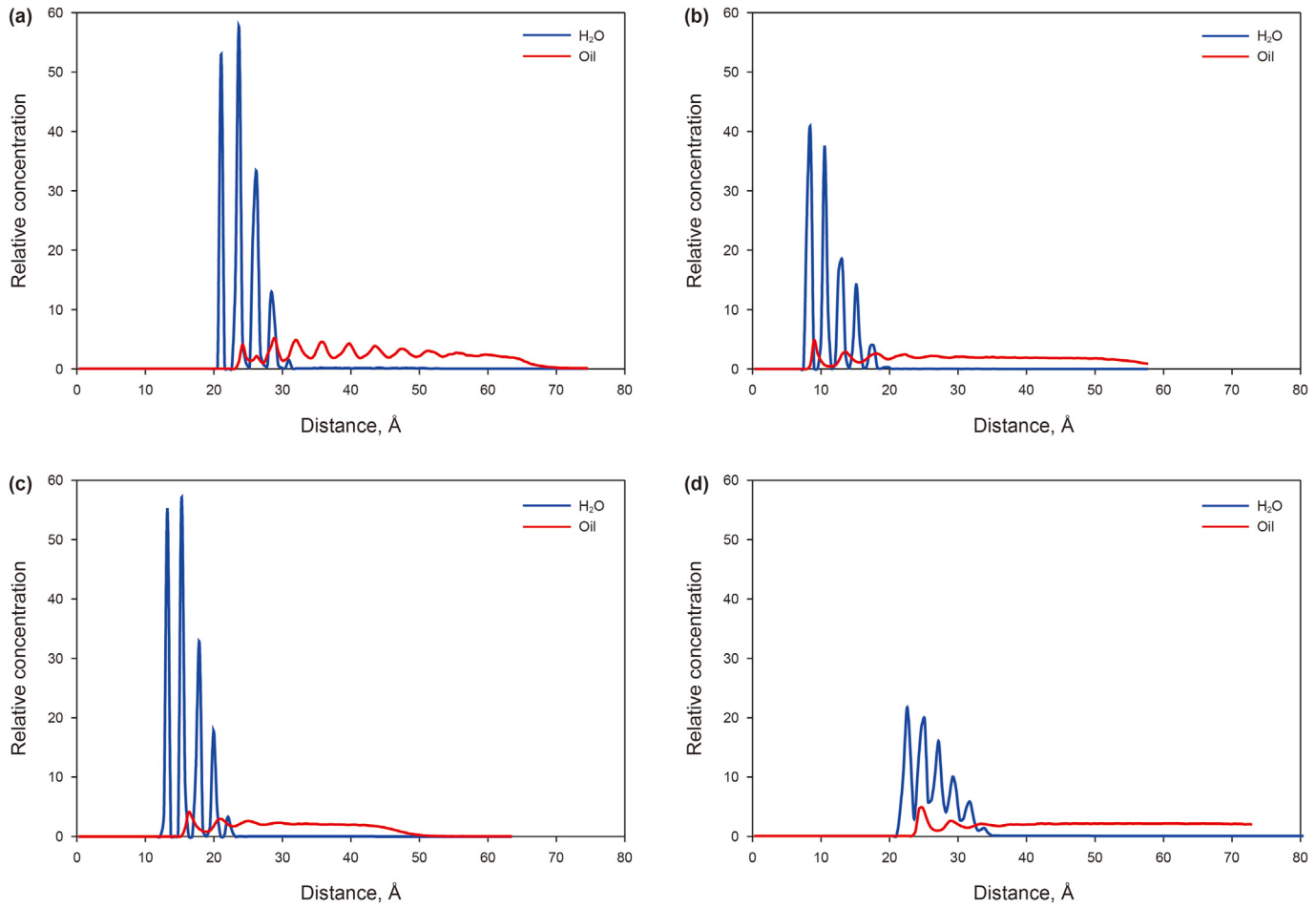


Fig. 5. Distribution of the oil and water concentrations in clay mineral wetting systems in *n*-hexane. (a) montmorillonite system; (b) kaolinite system; (c) chlorite system; (d) illite system.

we measured the water-side contact angle formed by the nano water droplets on the illite surface to be about 39.8°, similar to the results obtained by Arif et al. (2020) using MD simulation. According to the relative concentration distribution characteristics, the first water adsorption layer was closer to the hydroxylated quartz surface than the first oil adsorption layer and had a higher concentration (Fig. 5d). This indicates that the hydrophilicity of the illite surface is stronger than its lipophilicity, which is due to the high layer charge on the illite surface. These results are the same as those obtained by Zhang et al. (2016) using MD simulation to study the contact of "illite–water–alkane".

$$E_C = nE_A - E_B \tag{5}$$

where E_C is cohesive energy; n is the number of molecules of the system; E_A is the energy of a single molecule; E_B is the energy of the system.

The stronger the water wettability of a rock surface, the higher the relative concentration of surface water (Chang et al., 2018). According to the wetting process of the water droplets and the relative concentration curves of water on different mineral surfaces (Figs. 4 and 5), we can conclude that at 298 K, the hydrophilicity of the surfaces of the clay minerals in *n*-hexane follows the order montmorillonite > chlorite > kaolinite > illite. Moreover, most clay minerals showed strong water wettability. This is because most clay minerals are polar minerals, and there is a strong interaction between clay minerals and polar water molecules. In comparison, alkanes in shale oil are mostly nonpolar molecules. There is a weak van der Waals force between alkanes and reservoir minerals; thus, the interaction force between them is weak (Siddiqui and Chaudhry, 2018).

3.2. Radial distribution function (RDF)

We calculated the RDF between atoms in the structure of clay minerals and H_2O (Fig. 6) to explore possible high-energy adsorption sites on the surface of minerals. RDF usually refers to the spatial distribution probability of other particles given the coordinates of a particle, which can be used to describe the correlation of electrons and the affinity between two particles (Trokhymchuk et al., 2006; Amirhossein et al., 2021).

$$RDF = \frac{[n(r)]}{4\pi\rho r^2 \Delta r} = \frac{V}{N^2}\left[\sum_i \sum_{j\neq i}^{N} \delta(r - r_{ij})\right] \tag{6}$$

In this equation, r is a pair of radial distances from clay mineral molecules (Å); V is the capacity of the spherical shell (m^3); N is the number of particles; $[n(r)]$ is a function of the thickness of calculating the number of particles in a shell; and ρ is the average number density of particles (N/v).

As shown in Fig. 6a, the close contact peak between H_2O and K atoms in montmorillonite is sharper than that between H_2O and other atoms. This indicates that the substitution site around the K

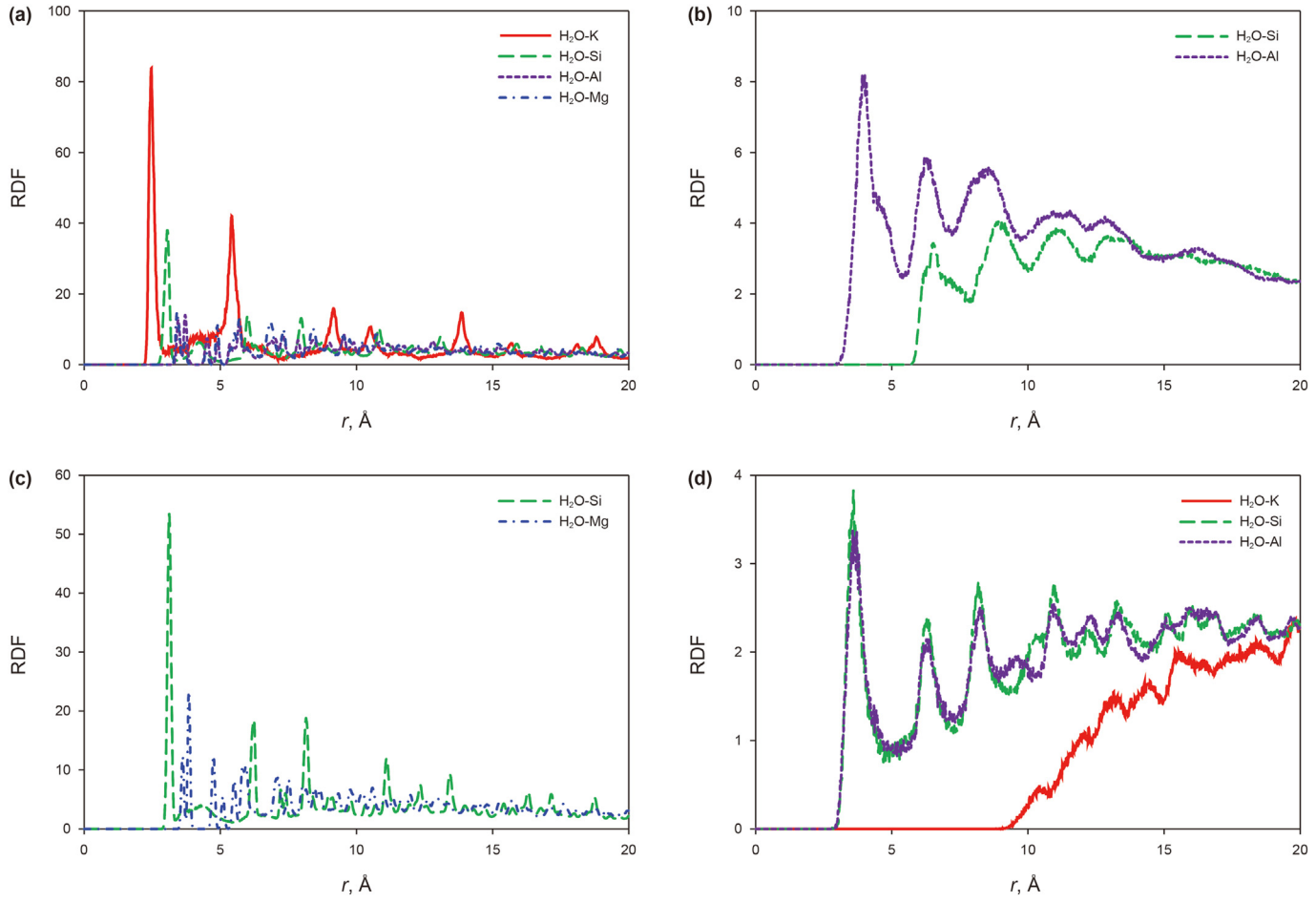


Fig. 6. RDF between H_2O and the atoms in the clay minerals. (a) montmorillonite; (b) kaolinite; (c) chlorite; (d) illite.

atoms in montmorillonite is the high-energy site of H_2O molecules. In Fig. 6b, the close contact peak between H_2O and Al atoms in kaolinite is sharper than that between H_2O and Si atoms. This indicates that the substitution site around the Al atoms in kaolinite is the high-energy site of H_2O molecules. In Fig. 6c, the close contact peak between H_2O and Si atoms in chlorite is sharper than that between H_2O and Mg atoms. This indicates that the substitution site around the Si atoms in chlorite is the high-energy site of H_2O molecules. In Fig. 6d, the close contact peak between H_2O and Si and Al atoms in illite is sharper than that between H_2O and K atoms. This indicates that the substitution sites around the Si and Al atoms in illite are the high-energy sites of H_2O molecules.

The higher the peak in RDF, the stronger the interaction between hydrocarbon molecules and clay mineral surfaces (Wang and Liang, 2019). Fig. 6 shows the following hydrophilicity order of water in *n*-hexane on the surfaces of clay minerals: montmorillonite > chlorite > kaolinite > illite.

3.3. Interaction energy

We took the last moment of the MD simulation (1000 ps) to calculate the interaction energy between *n*-hexane and water and the clay mineral surfaces and the difference between them to quantitatively evaluate the interaction between liquid hydrocarbon and water and clay mineral surface (Fig. 7). The interaction energy (E_{O-S}) between the *n*-hexane molecule and the clay mineral surface can be defined as follows (Chang et al., 2018; Zhong et al., 2013; Ma et al., 2019):

$$E_{O-S} = E_{O+S} - E_O - E_S \quad (7)$$

E_{O+S} is the total energy of the *n*-hexane molecule and the clay mineral surface (kcal/mol), E_O is the energy of the *n*-hexane molecule (kcal/mol), and E_S is the surface energy of clay minerals (kcal/mol).

The interaction energy (E_{w-s}) between the clay mineral surface and the water molecules can be defined as follows:

$$E_{W-S} = E_{W+S} - E_W - E_S \quad (8)$$

E_{W+S} is the total energy of the water molecules and clay mineral surface (kcal/mol), E_W is the energy of the water molecules (kcal/mol).

The interaction energy difference (ΔE) between E_{O-S} and E_{W-S} described by the following equation:

$$\Delta E = E_{O-S} - E_{W-S} \quad (9)$$

Fig. 7a shows the interaction energy of water and oil on different clay mineral surfaces. The greater the interaction energy between water and the clay mineral surface, the stronger the water wettability of the mineral (Chang et al., 2018). Therefore, it can be concluded from Fig. 7a that the hydrophilicity of the clay minerals is as follows: montmorillonite > chlorite > kaolinite > illite. The results show that ΔE on the surface of a water-wet rock is positive (Chang et al., 2018; Zhong et al., 2013). Fig. 7b shows the interaction energy difference (ΔE) between E_{O-S} and E_{W-S} of the different clay minerals in the steady state. It can be seen that ΔE is positive,

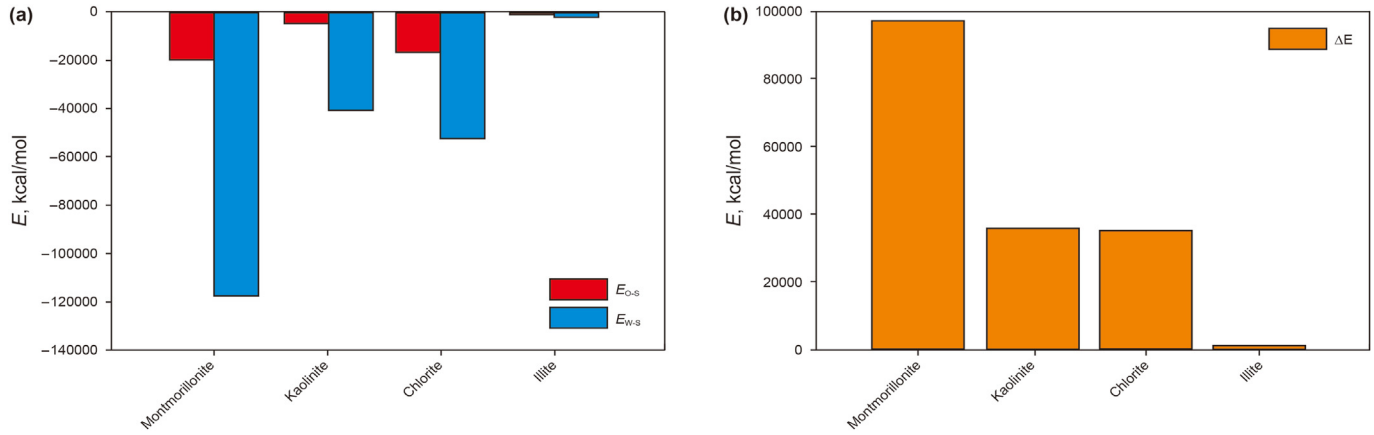


Fig. 7. Difference in interaction energy (a) between liquid hydrocarbons and water and the clay mineral surfaces and (b) between $E_{o\text{-}s}$ and $E_{w\text{-}s}$ of the different clay minerals in the steady state.

indicating that the interaction energy between the water molecules and the surfaces of the four clay minerals is greater than that between *n*-hexane and the surfaces of the clay minerals. The above discussion shows that $E_{W\text{-}S}$ and ΔE can well explain the different wettabilities of the clay mineral surfaces studied.

4. Discussion

4.1. Stability analysis

4.1.1. Change in kinetic energy

Kinetic energy is generally characterized the equilibrium state of a system (Zhong et al., 2013). The "montmorillonite, kaolinite, chlorite, and illite–water–*n*-hexane" wettability model and the evolution of kinetic energy in "montmorillonite, kaolinite, chlorite, and illite-water-toluene" are shown in Fig. 8. When the simulation reached 10 and 20 ps, each group of simulations attained balance (Fig. 8). This shows that the studied "oil–water–clay mineral" system stabilized.

4.1.2. Mean square displacement (MSD) and self-diffusion coefficient (D)

In this study, the movement characteristics of water molecules on the mineral surfaces were analyzed by calculating the *MSD* and *D* of water (Chakraborty et al., 2015; Tirjoo et al., 2019).

$$MSD = \frac{1}{N}\sum_{i=1}^{N}\left[r_i(t) - r_i(0)\right]^2 \tag{10}$$

$$D = \frac{1}{6N}\lim_{t\to\infty}\frac{\mathrm{d}}{\mathrm{d}t}\sum_{i=1}^{N}\left[r_i(t) - r_i(0)\right]^2 = \frac{1}{6}K_{MSD} \tag{11}$$

N is the number of diffusion molecules, $r_i(t)$ and $r_i(0)$ are the position vectors of the molecules at *t* and $t = 0$, respectively, and K_{MSD} is the slope of the *MSD* curve.

The *MSD* changes of the water molecules on the clay minerals are shown in Fig. 9. The relatively stable simulation data of the first 400 ps were selected for analysis (Yuan et al., 2021). With increasing simulation time, the value of *MSD* increases, but its slope decreases. This is because in the early stages of the simulation, the adsorption capacity of minerals for water was very large. Thus, the self-diffusion coefficient was also high. In the later stages, only a small part of the nonadsorbed water molecules moved, and the natural self-diffusion coefficient was small (Amirhossein et al., 2021). Fig. 9 shows that the self-diffusion coefficient of water in *n*-hexane and toluene on the surface of different clay minerals remained unchanged after about 300 ps. This indicates that the studied "oil–water–clay mineral" system stabilized.

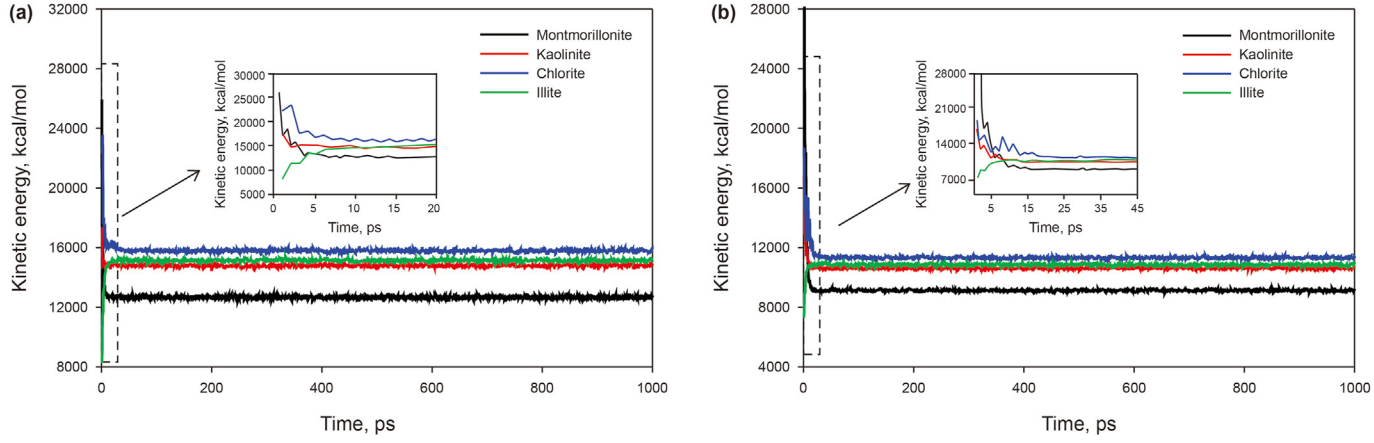


Fig. 8. Kinetic energy change diagram of each clay mineral wettability model in (a) *n*-hexane and (b) toluene.

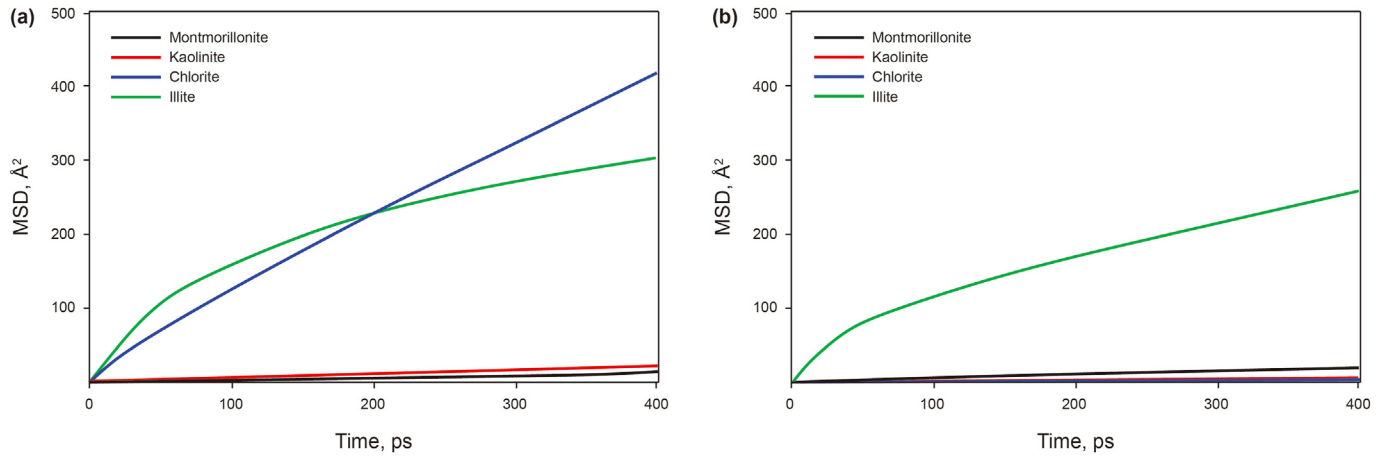


Fig. 9. Variation curve of the mean square displacement of the water molecules on the surfaces of clay minerals in (a) *n*-hexane; (b) toluene.

4.2. Force analysis

MD simulation is mainly based on the atomic force field model (Seyyedattar et al., 2019), which calculates the potential energy of the system through the functional form provided by the force field (Ebrahimi, 2014). The Lennard-Jones potential produced by the van der Waals and repulsive force interactions has been widely used because of its simple calculation (Lennard-Jones, 1924). When the distance is infinite, the potential of two particles is zero, which means that they do not interact. When the van der Waals force produces a rather weak gravitational force, the two particles may approach each other with the smallest energy. When the potential energy passes through zero, the atom reaches equilibrium. With the overlap of atomic electron clouds, the distance between two

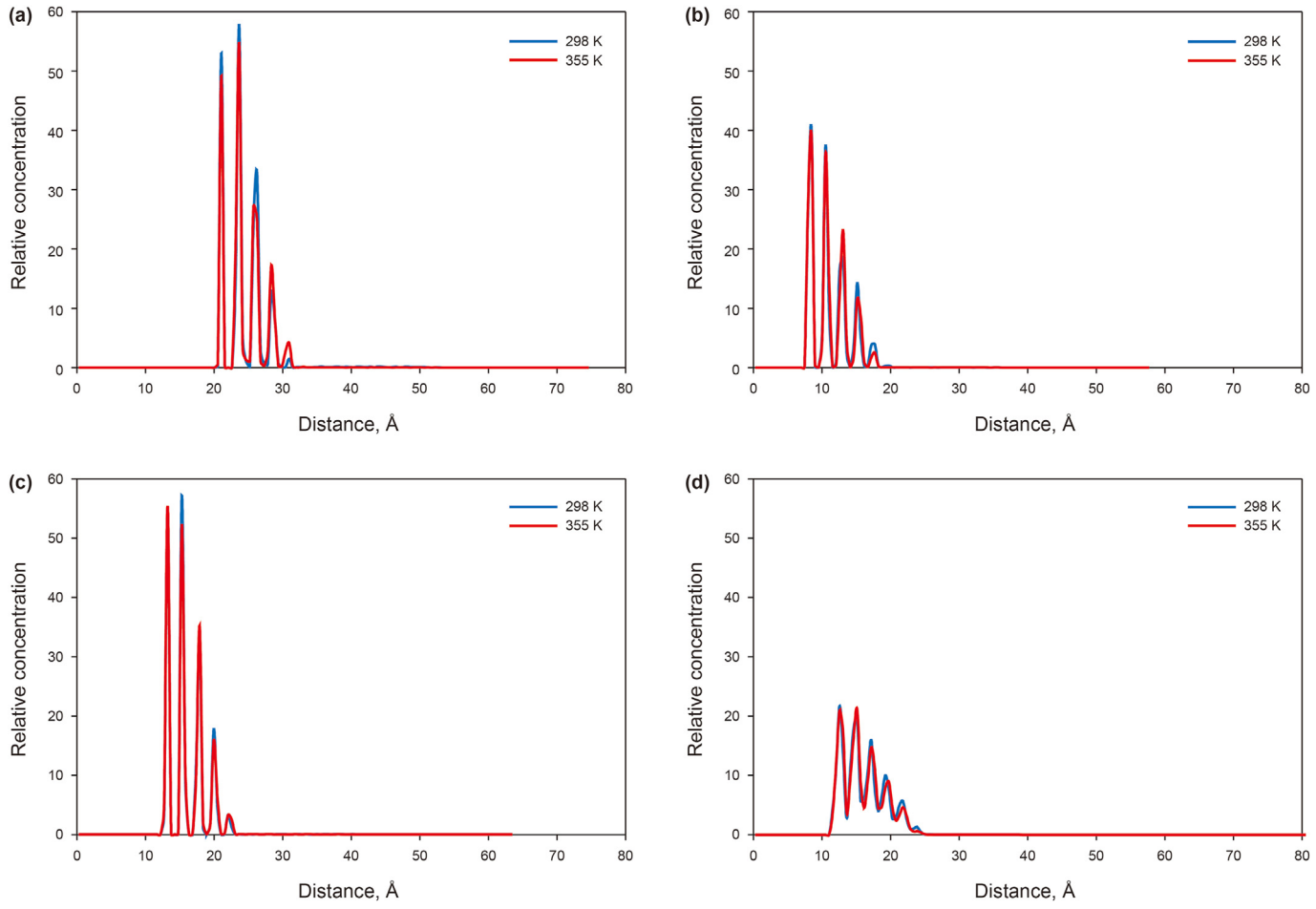


Fig. 10. Relative concentration of water in *n*-hexane on the surfaces of clay minerals at different temperatures. (a) montmorillonite; (b) kaolinite; (c) chlorite; (d) illite.

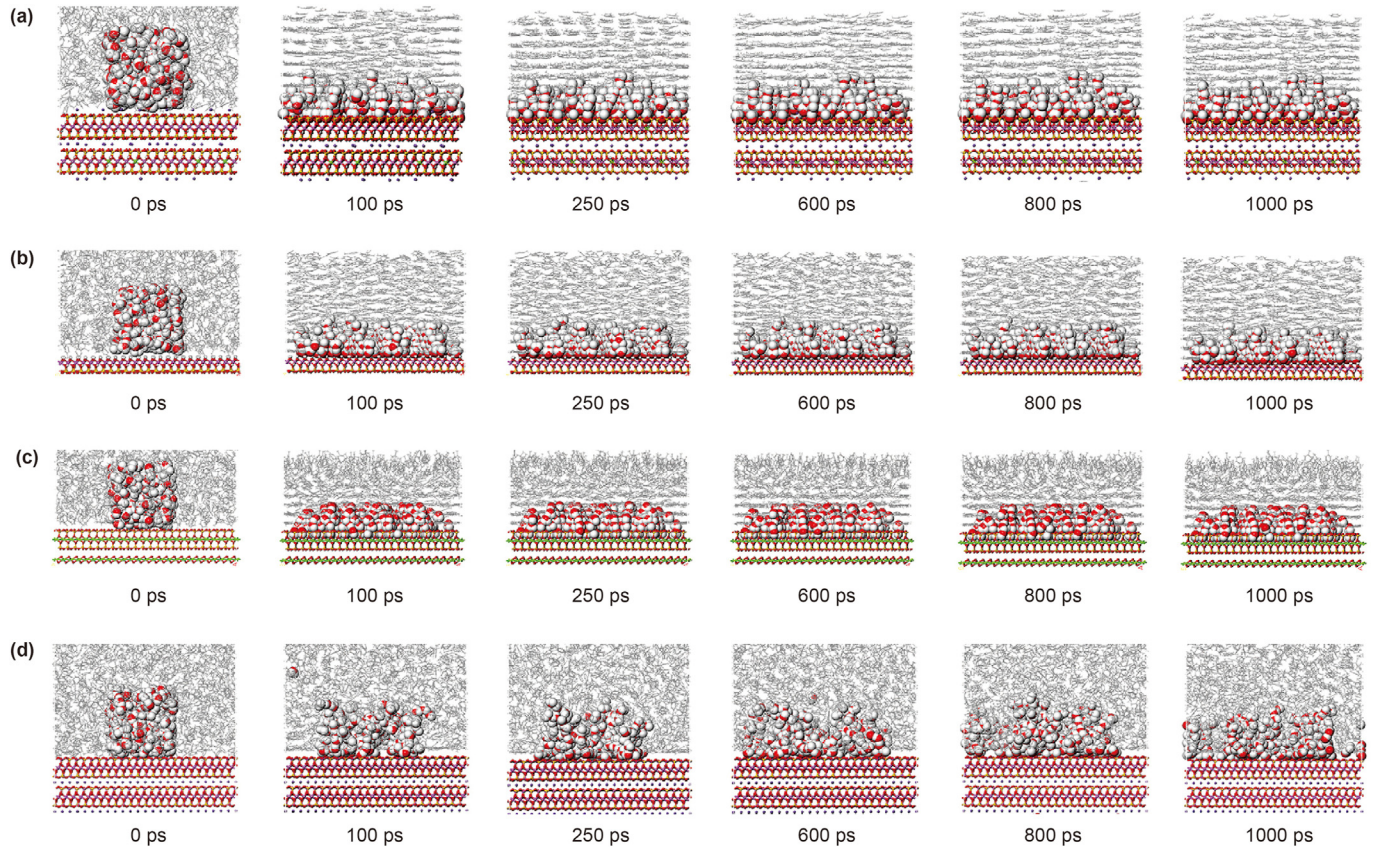


Fig. 11. Simulation screenshot of the oil–water wettability of clay minerals in toluene. (a) montmorillonite; (b) kaolinite; (c) chlorite; (d) illite.

particles is further reduced, resulting in strong repulsion. Consequently, the potential energy of the system suddenly increases (Ebrahimi, 2014; Seyyedattar et al., 2019).

The peak concentration of the adsorption layer gradually decreases with the increase of the distance from the mineral surface, and there is no obvious adsorption layer outside the distance of 10 Å from the mineral surface (Figs. 5 and 7). This shows that the intermolecular force between molecules dominates at a long distance from the mineral surface.

In 1873, Johannes Diderik van der Waals first introduced the concept of the van der Waals force (Klein, 1974). This force is meaningful only when atoms or molecules are very close. The fluctuations in atomic electron clouds allows atom to have instantaneous dipole moments, which induce nearby atoms to produce dipole moments, resulting in attractive dipole interactions (Visser, 1989). In addition to distance, the van der Waals force is also affected by polarity. Toluene has a high molecular weight in the liquid hydrocarbons, giving it a high van der Waals force. This may be the reason why the concentration of toluene on the surfaces of the clay minerals was higher than that of *n*-hexane.

The electrostatic force occurs between two charged particles, repels particles with the same charge and attracts particles with the opposite charge (Cao et al., 2020). The charge varies with the composition of clay minerals and liquid hydrocarbons, resulting in different electrostatic forces in different models. In our study, the charges of the clay minerals and the liquid hydrocarbon components were fixed. Thus, the distance became the main factor determining the electrostatic force, which increased with the decreasing distance between clay minerals and oil.

4.3. Analysis of the influencing factors on wettability

The clay mineral wettability is affected by many factors, including temperature, pressure, type of liquid hydrocarbon, and water salinity. Among these, small changes in pressure almost negligibly change the wettability (Seyyedi and Sohrabi, 2015; Najafi et al., 2016).

4.3.1. Effect of temperature on wettability

MD was used to simulate the relative concentration of water in *n*-hexane on the surface of different clay minerals at 298 K and 355 K to characterize the effect of temperature on wettability (Fig. 10). The concentration of water on the surfaces of montmorillonite, kaolinite, and illite decreased with increasing temperature, and the water wettability decreased. The concentration of water on the surface of chlorite increased with increasing temperature, and the water wettability increased. These results show that temperature changes have a certain effect on the wettability of clay minerals and are similar to the experimental results measured using the capture method (Alyaseri et al., 2017; Yekeen et al., 2021).

4.3.2. Effect of liquid hydrocarbon type on wettability

We established four “toluene–water–clay minerals” wettability models and made their oil-water concentration distribution diagrams to study the wettability in different liquid hydrocarbon components (Figs. 11 and 12). First, according to the wetting process of water droplets and the relative concentration curve of water on different mineral surfaces, we can conclude that at 298 K, the hydrophilicity of the surfaces of the clay minerals in toluene follows

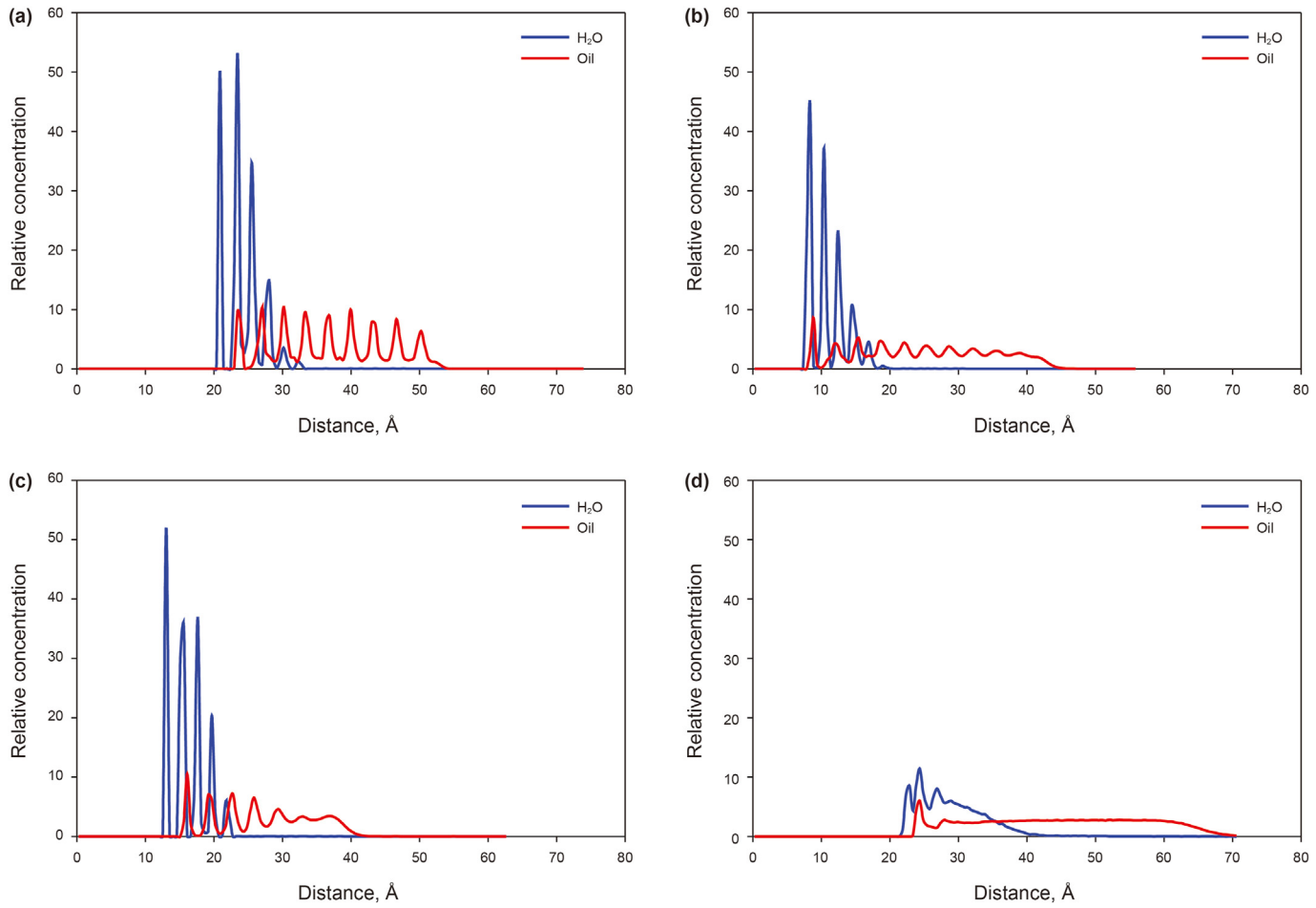


Fig. 12. Distribution of the oil–water concentration in each clay mineral wetting system in toluene. (a) montmorillonite; (b) kaolinite; (c) chlorite; (d) illite.

the order montmorillonite > chlorite > kaolinite > illite, which is the same as that of the clay minerals in *n*-hexane. Second, Fig. 11 shows that the water in toluene is not completely paved on the surfaces of montmorillonite, kaolinite, chlorite, and illite. Fig. 12 shows that the relative concentration of water on the surfaces of the clay minerals decreased and the relative concentration of oil increased. These indicate that the water in toluene had weaker water wettability and stronger oil wettability than those of the water in *n*-hexane on the surfaces of the clay minerals. Therefore, the liquid hydrocarbon type also has a certain influence on the wettability of clay minerals (Chang et al., 2018).

4.3.3. *Effect of water salinity on wettability*

Illite with relatively poor water wettability was selected to establish a wettability model to more intuitively observe the changes in water with different mineralization on the surface of clay minerals. Three different concentrations of $NaHCO_3$ in water droplets were established using the molecular dynamics method: 300 water molecules at 10, 20, and 40 $NaHCO_3$, respectively. We established the "illite–*n*-hexane–$NaHCO_3$" wettability model, simulated it at 1000 ps under the NVT and at 298 K, and took screenshots of the models at different simulation times (Fig. 13). We found that with increasing $NaHCO_3$ concentrations, the adhesion of water on the mineral surfaces lessened (Fig. 13), gradually becoming miscible with *n*-hexane, and the relative concentration on the mineral surface continuously decreased (Fig. 14). Therefore, the higher the $NaHCO_3$ concentration in water, the weaker the wettability of the clay mineral surfaces to water. Therefore, the salinity of water also has a certain impact on the wettability of clay minerals (Chang et al., 2018).

During the extraction of shale oil, the changes of temperature, pressure and fluid properties will affect the wettability. The influence of temperature and pressure on wettability is very complex. Generally, in the process of shale oil exploitation, the formation energy will gradually decrease, the pressure and temperature will gradually decrease, the crude oil viscosity will increase, the oil wettability will increase, and the water wettability will weaken (Li, 2021).

4.4. *Shortcomings and deficiencies*

Because most clay minerals in shale have strong hydrophilicity, the water molecules completely spread on the mineral surface during the simulation (Figs. 4 and 11). Thus, measuring the specific value of the contact angle using the contact angle measurement method for wettability comparisons is impossible. Only indirect parameters can be used for wettability evaluation.

Alkanes cannot fully represent shale oil. We tried to simulate shale oil with molecular dynamics before, but found that the complexity of shale oil components makes the simulation workload and difficulty very large. We investigated the relevant literature and found that in recent years, many scholars have used the high content of alkanes in shale oil to represent shale oil for molecular simulation (Wang et al., 2016; Cao et al., 2020; Dong et al., 2022;

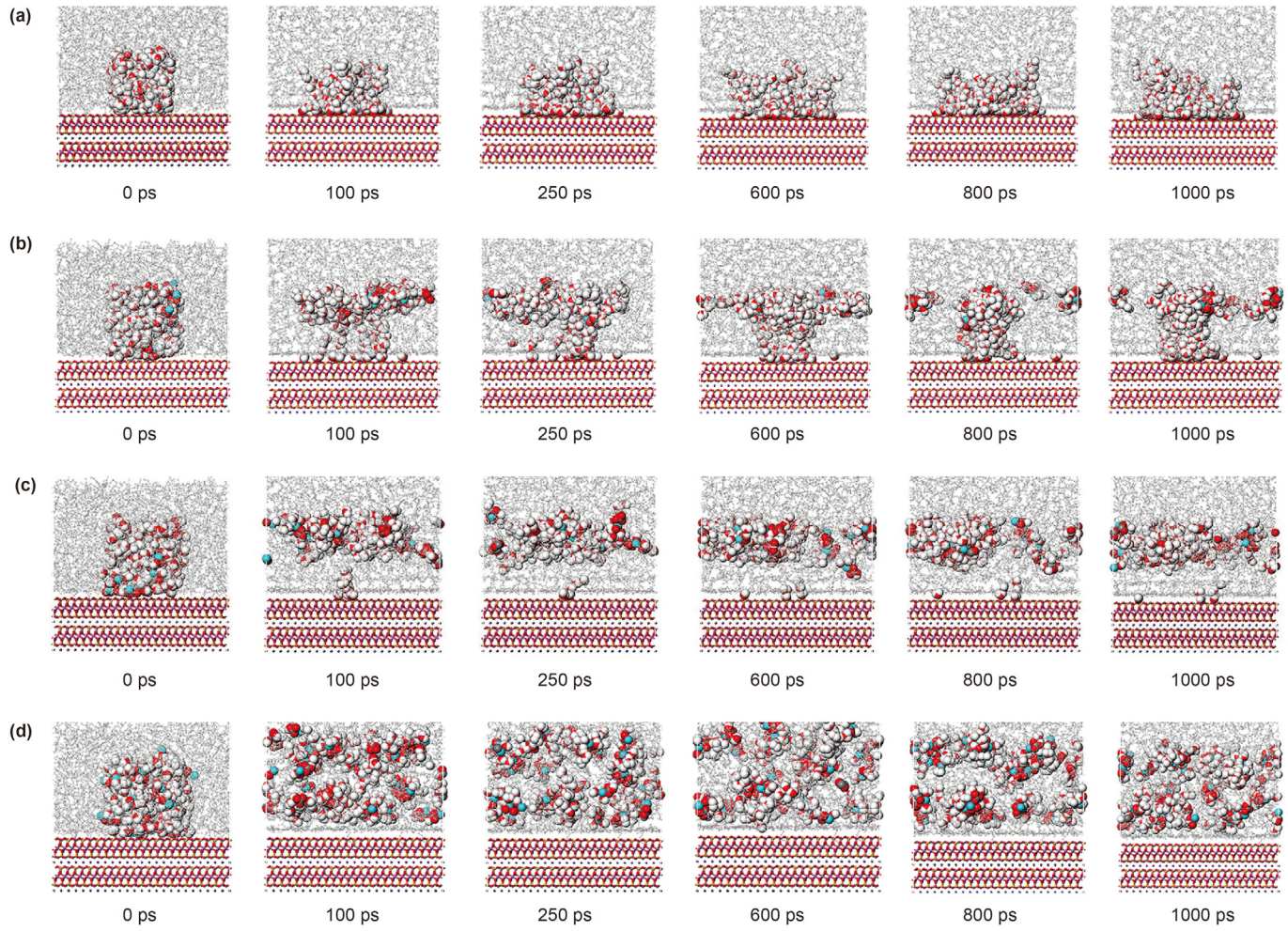


Fig. 13. Wettability model of illite with different $NaHCO_3$ concentrations. (a) 300 H_2O and 0 $NaHCO_3$; (b) 300 H_2O and 10 $NaHCO_3$; (c) 300 H_2O and 20 $NaHCO_3$; (d) 300 H_2O and 40 $NaHCO_3$.

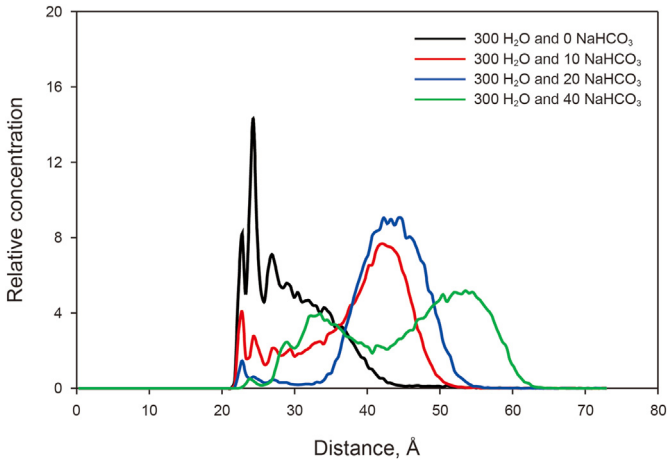


Fig. 14. Relative $NaHCO_3$ concentrations of water droplets with different concentrations on the surfaces of illite.

Sang et al., 2022). Therefore, this manuscript uses two hydrocarbon components (*n*-hexane and toluene) with high content in shale oil to study the wettability of clay minerals. Although shale oil simulation is a difficulty, it will be the main task of our future work.

We used the MD simulation method to comprehensively analyze the change form and relative concentration of water on the surfaces of different minerals, the RDF of water and clay mineral surface atoms, and the interaction energy between water and the clay minerals surface. Finally, the wettability of four common clay mineral surfaces in shale were obtained, which are of breakthrough significance. However, this still cannot represent the actual wettability situations of underground clay minerals. Thus, we must obtain the relative content of each clay mineral component in shale through X-ray diffraction analysis, accordingly give each mineral a certain proportion, simulate actual underground temperatures, pressures, mineral surface roughness and fluid mineralization, and finally conduct comprehensive analyses. Only in this way can we really simulate the wettability of clay minerals in underground shale, which will be the main direction of our future research.

5. Conclusions

(1) In this paper, using MD simulation, we microscopically analyzed the changing morphology and relative concentration of water on the surfaces of different clay minerals. The RDF of water and clay mineral surface atoms, the interaction energy between water and the clay mineral surfaces, and the inherent wettability of the montmorillonite, kaolinite, chlorite, and illite surfaces at the nanoscale was obtained. The

results show the following order of the water wettability of the clay minerals: montmorillonite > chlorite > kaolinite > illite. The simulation results are consistent with the experimental results, which well proves the accuracy of the MD simulation.

(2) It is concluded that the temperature, type of liquid hydrocarbon, and mineralization of water all have a certain influence on wettability. The water wettability of montmorillonite, kaolinite, and illite decreased with increasing temperature. In contrast, the water wettability of chlorite increased with increasing temperature. The water in toluene had weaker water wettability and stronger oil wettability than that in *n*-hexane on the surfaces of the clay minerals. The higher the $NaHCO_3$ concentration, the weaker the wettability of the clay mineral surface to water.

Declaration of competing interest

The authors declare that they have no known competing financial interests or personal relationships that could have appeared to influence the work reported in this paper.

Acknowledgements

This work was supported by the National Natural Science Foundation of China (Grant number 42102145; 41872148); the Science Foundation of China University of Petroleum, Beijing (Grant number 2462020BJRC005; 2462022YXZZ007); AAPG Foundation Grants-in-Aid Program (Grant number 22108817); and the Joint Fund of the National Natural Science Foundation of China (Grant number U19B6003-02-04).

Appendix A. Supplementary data

Supplementary data to this article can be found online at https://doi.org/10.1016/j.petsci.2023.02.001.

References

Al-Garadi, K., El-Husseiny, A., Elsayed, M., et al., 2022. A rock core wettability index using NMR T_2 measurements. J. Petrol. Sci. Eng. 208, 109386. https://doi.org/10.1016/j.petrol.2021.109386.

Al-Shafei, M.A., Okasha, T.M., 2009. Wettability studies at the pore level of Saudi aramco reservoirs. Spe Saudia Arabia. https://doi.org/10.2118/126088-MS.

Alvarez, J.O., Schechter, D.S., 2016. Application of wettability alteration in the exploitation of unconventional liquid resources. Petrol. Explor. Dev. 43, 832–840. https://doi.org/10.1016/S1876-3804(16)30099-4.

Al-Yaseri, A., Yekeen, N., Al-Mukainah, H.S., et al., 2022. Rock-wettability impact on CO_2-carbonate rock interaction and the attendant effects on CO_2 storage in carbonate reservoirs. J. Nat. Gas Sci. Eng. 104, 104664. https://doi.org/10.1016/j.jngse.2022.104664.

Alyaseri, A.Z., Roshan, H., Zhang, Y., et al., 2017. Effect of the temperature on CO_2/brine/dolomite wettability: hydrophilic versus hydrophobic surfaces. Energy Fuel. 31, 6329–6333. https://doi.org/10.1021/acs.energyfuels.7b00745.

Amirhossein, F.F., Abdolnabi, H., Ghasem, Z., et al., 2021. Molecular dynamics modeling and simulation of silicon dioxide-low salinity water nanofluid for enhanced oil recovery. J. Mol. Liq. 339, 116834. https://doi.org/10.1016/j.molliq.2021.116834.

Amott, E., 1958. Observations relating to the wettability of porous media. Trans Aime 216, 156–162. https://doi.org/10.1016/0502-8205(59)90017-6.

Andersen, Hans C., 1980. Molecular dynamics simulations at constant pressure and/or temperature. J. Chem. Phys. 72, 2384–2393. https://doi.org/10.1063/1.439486.

Anderson, William, G., 1986. Wettability literature survey-Part 3: the effects of wettability on the electrical properties of porous media. J. Petrol. Technol. 38, 1371–1378. https://doi.org/10.2118/13934-PA.

Arif, M., Abu-Khamsin, S.A., Zhang, Y.H., et al., 2020. Experimental investigation of carbonate wettability as a function of mineralogical and thermo-physical conditions. Fuel 264, 116846. https://doi.org/10.1016/j.fuel.2019.116846.

Babatunde, K.A., Negash, B.M., Mojid, M.R., et al., 2021. Molecular simulation study of CO_2/CH_4 adsorption on realistic heterogeneous shale surfaces. Appl. Surf. Sci. 543, 148789. https://doi.org/10.1016/j.apsusc.2020.148789.

Barclay, S.A., Worden, R.H., 2000. Effects of reservoir wettability on quartz cementation in oil fields. Quartz Cement Sandstones 29, 103–117. https://doi.org/10.1002/9781444304237.ch8.

Boneau, D.F., Clampitt, R.L., 1977. A surfactant system for the oil-wet sandstone of the north burbank unit. J. Petrol. Technol. 29 (5), 501–506. https://doi.org/10.2118/5820-PA.

Boyer, C., Kieschnick, J., Suarez-Rivera, R., et al., 2006. Producing gas from its source. Oilfield Rev. 18, 36–49.

Cao, Z., Jiang, H., Zeng, J.H., et al., 2020. Nanoscale liquid hydrocarbon adsorption on clay minerals: a molecular dynamics simulation of shale oils. Chem. Eng. J. 420, 127578. https://doi.org/10.1016/j.cej.2020.127578.

Chakraborty, T., Hens, A., Kulashrestha, S., et al., 2015. Calculation of diffusion coefficient of long chain molecules using molecular dynamics. Phys. E Low-dimens. Syst. Nanostruct. 69, 371–377. https://doi.org/10.1016/j.physe.2015.01.008.

Chang, X., Xue, Q.Z., Li, X.F., et al., 2018. Inherent wettability of different rock surfaces at nanoscale: a theoretical study. Appl. Surf. Sci. 434, 73–81. https://doi.org/10.1016/j.apsusc.2017.10.173.

Chen, Y.Q., Ubaidah, A., Elakneswaran, Y., et al., 2020. Detecting pH and Ca^{2+} increase during low salinity waterflooding in carbonate reservoirs: implications for wettability alteration process. J. Mol. Liq. 317, 114003. https://doi.org/10.1016/j.molliq.2020.114003.

Chilingar, G.V., Yen, T.F., 1983. Some notes on wettability and relative permeabilities of carbonate reservoir rocks, II. Energy Sources 7 (1), 67–75. https://doi.org/10.1080/00908318308908076.

Donaldson, E.C., Thomas, R.D., Lorenz, P.B., 1969. Wettability determination and its effect on recovery efficiency. SPE J. 9, 13–20. https://doi.org/10.2118/2338-PA.

Dong, H., Zhou, Y., Zheng, C., et al., 2021. On the role of the amphiphobic surface properties in droplet wetting behaviors via molecular dynamics simulation. Appl. Surf. Sci. 544, 148916. https://doi.org/10.1016/j.apsusc.2020.148916.

Dong, X.H., Xu, W.J., Liu, R.J., et al., 2022. Insights into adsorption and diffusion behavior of shale oil in slit nanopores: a molecular dynamics simulation study. J. Mol. Liq. 359 (1), 119322. https://doi.org/10.1016/j.molliq.2022.119322.

Du, H., Miller, J.D., 2007. A molecular dynamics simulation study of water structure and adsorption states at talc surfaces. Int. J. Miner. Process. 84, 172–184. https://doi.org/10.1016/j.minpro.2006.09.008.

Ebrahimi, D., 2014. Multiscale Modeling of Clay-Water Systems. Massachusetts Institute of Technology.

Edward, Bormashenko, 2018. Apparent contact angles for reactive wetting of smooth, rough, and heterogeneous surfaces calculated from the variational principles. J. Colloid Interface Sci. 537, 597–603. https://doi.org/10.1016/j.jcis.2018.11.068.

Ehrenberg, S.N., Skjevrak, I., Gilje, A.E., 1995. Asphaltene-rich residues in sandstone reservoirs of Haltenbanken province, mid-Norwegian continental shelf. Mar. Petrol. Geol. 12 (1), 53–69. https://doi.org/10.1016/0264-8172(95)90387-Y.

El-Shater, A., Mansour, A.M., Osman, M.R., et al., 2021. Evolution and significance of clay minerals in the esna shale formation at dababiya area, luxor, Egypt. Egyptian Journal of Petroleum 30, 9–16. https://doi.org/10.1016/j.ejpe.2021.03.001.

Fan, C.F., Cagin, T., 1995. Wetting of crystalline polymer surfaces: a molecular dynamics simulation. J. Chem. Phys. 103. https://doi.org/10.1063/1.470016, 9053-9053.

Fassi-Fihri, O., Robin, M., Rosenberg, E., 1995. Wettability studies at the pore level: a new approach by the use of cryo-scanning electron microscopy. SPE Form. Eval. 10, 11–19. https://doi.org/10.2118/22596-pa, 01.

Gao, Z.Y., Hu, Q.H., 2018. Pore structure and spontaneous imbibition characteristics of marine and continental shales in China. AAPG (Am. Assoc. Pet. Geol.) Bull. 102, 1941–1961. https://doi.org/10.1306/03291817297.

Gualtieri, A.F., 2000. Accuracy of XRPD QPA using the combined Rietveld–RIR method. J. Appl. Crystallogr. 33, 267–278. https://doi.org/10.1107/S002188989901643X.

Guo, R.C., Dalton, L., Crandall, D., et al., 2022. Role of heterogeneous surface wettability on dynamic immiscible displacement, capillary pressure, and relative permeability in a CO2-water-rock system. Adv. Water Resour. 165, 104226. https://doi.org/10.1016/j.advwatres.2022.104226.

Heinz, H., Koerner, H., Anderson, K.L., et al., 2005. Force field for mica-type silicates and dynamics of octadecylammonium chains grafted to montmorillonite. Chem. Mater. 17, 5658–5669. https://doi.org/10.1021/cm0509328.

Heydari, M., Sharif, F., Ebrahimi, M., 2021. A molecular dynamics study on the role of oxygen-containing functional groups on the adhesion of polymeric films to the aluminum surface. Fluid Phase Equil. 536, 112966. https://doi.org/10.1016/j.fluid.2021.112966.

Hou, J.J., Lin, S.L., Zhang, M., et al., 2022. Salinity, temperature and pressure effect on hydrogen wettability of carbonate rocks. Int. J. Hydrogen Energy. https://doi.org/10.1016/j.ijhydene.2022.05.274.

Hu, T., Pang, X.Q., Xu, T.W., et al., 2022a. Identifying the key source rocks in heterogeneous saline lacustrine shales: paleogene shales in the Dongpu depression, Bohai Bay Basin, eastern China. AAPG (Am. Assoc. Pet. Geol.) Bull. 106, 1325–1356. https://doi.org/10.1306/01202218109.

Hu, T., Pang, X.Q., Jiang, F.J., et al., 2022b. Dynamic continuous hydrocarbon accumulation (DCHA): existing theories and a new unified accumulation model. Earth Sci. Rev. 232, 104109. https://doi.org/10.1016/j.earscirev.2022.104109.

Hu, Y., Devegowda, D., Sigal, R., 2016. A microscopic characterization of wettability in shale kerogen with varying maturity levels. J. Nat. Gas Sci. Eng. 33, 1078–1086. https://doi.org/10.1016/j.jngse.2016.06.014.

Jarvie, D.M., 2012. Shale resource systems for oil and gas: Part 1—shale-gas

resource systems. AAPG Memoir 97, 69–87. https://doi.org/10.1306/13321446M973489.
Jin, Z.J., Bai, Z.R., Gao, B., et al., 2019. Has China ushered in the shale oil and gas revolution? Oil Gas Geol. 40, 451–458 (in Chinese).
Klein, M.J., 1974. The historical origins of the Van der Waals equation. Physica 73, 28–47. https://doi.org/10.1016/0031-8914(74)90224-9.
Lan, Q., Xu, M., Dehghanpour, H., et al., 2014. Advances in understanding wettability of tight and shale gas formations. In: SPE Annual Technical Conference and Exhibition. https://doi.org/10.2118/170969-ms.
Law, B.E., Curtis, J.B., 2002. Introduction to unconventional petroleum systems. AAPG (Am. Assoc. Pet. Geol.) Bull. 86, 1851–1852. https://doi.org/10.1306/61EEDDA0-173E-11D7-8645000102C1865D.
Lennard-Jones, J.E., 1924. On the determination of molecular fields. II. From the equation of state of gas. Proc. Roy. Soc. Lond. 106, 463–477.
Li, J., Wang, F., 2017. Water graphene contact surface investigated by pairwise potentials from force-matching PAW-PBE with dispersion correction. J. Chem. Phys. 146, 054702. https://doi.org/10.1063/1.4974921.
Li, K., Xi, K.L., Cao, Y.C., et al., 2021. Chlorite authigenesis and its impact on reservoir quality in tight sandstone reservoirs of the Triassic Yanchang Formation, southwestern Ordos Basin, China. J. Petrol. Sci. Eng. 205, 108843. https://doi.org/10.1016/j.petrol.2021.108843.
Li, M.W., Jin, Z.J., Dong, M.Z., et al., 2020. Research Progress on formation and evolution of continental shale and shale oil enrichment mechanism. Petrol. Geol. Exp. 42, 489–505 (in Chinese).
Li, P., 2021. Wettability of Shale and its Effect on Methane Adsorption : A Case Study of Shanxi and Taiyuan Formations in Southern North China Basin. China University of Geosciences, Beijing), Beijing. https://doi.org/10.27493/d.cnki.gzdzy.2021.000053.
Lister, J.S., Bailey, S.W., 1967. Chlorite polytypism: IV. Regular two-layer structures refined structure. Am. Mineral. 52, 1614–1631.
Liu, G.F., Yin, H., Lan, S.X., et al., 2020. Experimental determination of dynamic pore-throat structure characteristics in a tight gas sandstone formation with consideration of effective stress. Mar. Petrol. Geol. 113, 104170. https://doi.org/10.1016/j.marpetgeo.2019.104170.
Lu, S.F., Xue, H.T., 2021. Formation Conditions, Occurrence Mechanism and Enrichment Distribution of Shale Oil. Petroleum Industry Press, Beijing (in Chinese).
Lu, X.C., Hou, Q.F., Yin, L., et al., 2003. Measurement and discussion of contact angle of several common minerals. Acta Petrol. Mineral. 397–400, 04 (in Chinese).
Luo, P., Zhong, N.N., Khan, I., et al., 2019. Effects of pore structure and wettability on methane adsorption capacity of mud rock: insights from mixture of organic matter and clay minerals. Fuel 251, 551–561. https://doi.org/10.1016/j.fuel.2019.04.072.
Ma, Y., Lu, G.W., Shao, C.J., et al., 2019. Molecular dynamics simulation of hydrocarbon molecule adsorption on kaolinite (0 0 1) surface. Fuel 237, 989–1002. https://doi.org/10.1016/j.fuel.2018.10.063.
Maurice, C.P., 1967. Fluid-release mechanisms in compacting marine mudrocks and their importance in oil exploration. AAPG (Am. Assoc. Pet. Geol.) Bull. 51. https://doi.org/10.1306/5d25c137-16c1-11d7-86450.
Mohammed, S., Gadikota, G., 2020. Dynamic wettability alteration of calcite, silica and illite surfaces in subsurface environments: a case study of asphaltene self-assembly at solid interfaces. Appl. Surf. Sci. 505, 144516. https://doi.org/10.1016/j.apsusc.2019.144516.
Morrow, N.R., 1990. Wettability and its effect on oil recovery. J. Petrol. Technol. 42, 1476–1484. https://doi.org/10.2118/21621-PA.
Najafi, A., Barati, A., Soleymanzadeh, A., et al., 2016. Experimental investigation of effect of temperature and pressure on contact angle of four Iranian carbonate oil reservoirs. J. Petrol. Sci. Eng. 142, 77–84. https://doi.org/10.1016/j.petrol.2016.02.004.
Omidi, M., Fatehinya, A., Farahani, M., et al., 2017. Characterization of biomaterials. Biomater. Oral and Dental Tissue Eng. 97–115. https://doi.org/10.1016/B978-0-08-100961-1.00007-4.
Pan, B., Jones, F., Huang, Z., et al., 2019. Methane (CH_4) wettability of clay-coated quartz at reservoir conditions. Energy Fuel. 33, 788–795. https://doi.org/10.1021/acs.energyfuels.8b03536.
Pan, B., Yin, X., Iglauer, S., 2020. A review on clay wettability: from experimental investigations to molecular dynamics simulations. Adv. Colloid Interface Sci. 285, 102266. https://doi.org/10.1016/j.cis.2020.102266.
Pham, A.V., Fang, T.H., Nguyen, V.T., et al., 2021. Impact and wetting properties of Au nanoparticle on Cu (001) textured surfaces by molecular dynamics. Mater. Chem. Phys. 272, 125039. https://doi.org/10.1016/j.matchemphys.2021.125039.
Salehi, M., Johnson, S.J., Liang, J.T., 2008. Mechanistic study of wettability alteration using surfactants with applications in naturally fractured reservoirs. Langmuir 24, 14099. https://doi.org/10.1021/la802464u.
Sang, Q., Zhao, X.Y., Liu, H.M., et al., 2022. Analysis of imbibition of n-alkanes in kerogen slits by molecular dynamics simulation for characterization of shale oil rocks. Petrol. Sci. 19 (3), 1236–1249. https://doi.org/10.1016/j.petsci.2022.01.005.
Scanziani, A., Singh, K., Blunt, M.J., et al., 2017. Automatic method for estimation of in situ effective contact angle from X-ray micro tomography images of two-phase flow in porous media. J. Colloid Interface Sci. 496, 51–59. https://doi.org/10.1016/j.jcis.2017.02.005.
Schmatz, J., Urai, J.L., Berg, S., et al., 2015. Nanoscale imaging of pore-scale fluid-fluid-solid contacts in sandstone: imaging Fluid-Fluid-Solid Contacts. Geophys. Res. Lett. 42 (7), 2189–2195. https://doi.org/10.1002/2015GL063354.
Seyyedattar, M., Zendehboudi, S., Butt, S., 2019. Invited review - molecular dynamics simulations in reservoir analysis of offshore petroleum reserves: a systematic review of theory and applications. Earth Sci. Rev. 192, 194–213. https://doi.org/10.1016/j.earscirev.2019.02.019.
Seyyedi, M., Sohrabi, M., 2015. Investigation of rock wettability alteration by carbonated water through contact angle measurements. Energy Fuel. 29, 5544–5553. https://doi.org/10.1021/acs.energyfuels.5b01069.
Shang, J., Flury, M., Harsh, J.B., et al., 2010. Contact angles of aluminosilicate clays as affected by relative humidity and exchangeable cations. Colloids Surf. A Physicochem. Eng. Asp. 353, 1–9. https://doi.org/10.1016/j.colsurfa.2009.10.013.
Shi, K.Y., Chen, J.Q., Pang, X.Q., et al., 2022. Effect of wettability of shale on CO_2 sequestration with enhanced gas recovery in shale reservoir: implications from molecular dynamics simulation. J. Nat. Gas Sci. Eng. 107, 104798. https://doi.org/10.1016/j.jngse.2022.104798.
Siddiqui, S.I., Chaudhry, S.A., 2018. A review on graphene oxide and its composites preparation and their use for the removal of As^{3+} and As^{5+} from water under the effect of various parameters: application of isotherm, kinetic and thermodynamics. Process Saf. Environ. Protect. 119, 138–163. https://doi.org/10.1016/j.psep.2018.07.020.
Singh, D., Roy, S., Pant, H.J., et al., 2022. A novel approach for wettability estimation in geological systems by fluid–solid interfacial area measurement using tracers. J. Petrol. Sci. Eng. 215, 110722. https://doi.org/10.1016/j.petrol.2022.110722.
Solc, R., Gerzabek, M.H., Lischka, H., et al., 2011. Wettability of kaolinite (001) surfaces-Molecular dynamic study. Geoderma 169, 47–54. https://doi.org/10.1016/j.geoderma.2011.02.004.
Steiner, T., Desiraju, G.R., 1998. Distinction between the weak hydrogen bond and the van der Waals interaction. Chem. Commun. 8, 891–892. https://doi.org/10.1039/A708099I.
Stumm, W., 1992. Chemistry of the Solid-Water Interface. Wiley, New York, p. 428.
Sun, H., 1998. COMPASS: an ab initio force-field optimized for condensed-phase applications—overview with details on alkane and benzene compounds. J. Phys. Chem. B 102, 7338–7364. https://doi.org/10.1021/jp980939v.
Tavakoli, D., Tarighat, A., 2016. Molecular dynamics study on the mechanical properties of Portland cement clinker phases. Comput. Mater. Sci. 119, 65–73. https://doi.org/10.1016/j.commatsci.2016.03.043.
Tirjoo, A., Bayati, B., Rezaei, H., et al., 2019. Molecular dynamics simulations of asphaltene aggregation under different conditions. J. Petrol. Sci. Eng. 177, 392–402. https://doi.org/10.1016/j.petrol.2019.02.041.
Trokhymchuk, A., Nezbeda, I., JirsaK, J., et al., 2006. Hard-sphere radial distribution function again. J. Chem. Phys. 123, 024501. https://doi.org/10.1063/1.2188941.
Visser, J., 1989. Van der Waals and other cohesive forces affecting powder fluidization. Powder Technol. 58, 1–10. https://doi.org/10.1016/0032-5910(89)80001-4.
Wang, F.H.L., Guidry, L.J., 1994. Effect of oxidation-reduction condition on wettability alteration. SPE Form. Eval. 9, 140–148. https://doi.org/10.2118/20504-pa, 02.
Wang, Q., Liang, H., 2019. Molecular insight into competitive adsorption of methane and carbon dioxide in montmorillonite: effect of clay structure and water content. Fuel 239, 32–43. https://doi.org/10.1016/j.fuel.2018.10.149.
Wang, S., Javadpour, F., Feng, Q.H., 2016. Molecular dynamics simulations of oil transport through inorganic nanopores in shale. Fuel 171 (1), 74–86. https://doi.org/10.1016/j.fuel.2015.12.071.
Wei, J.M., Yang, H.M., Zhu, J.X., et al., 2009. Molecular dynamic simulation on interlayer micro-structure in organic montmorillonite. Mineral. Petrol. 29, 33–37. https://doi.org/10.19719/j.cnki.1001-6872.2009.01.006, 2009.
Wu, C.Z., 2018. Molecular Dynamics Simulation of Shale Oil Occurrence Characteristics. China University of Petroleum. https://doi.org/10.27644/d.cnki.gsydu.2018.001747 (East China).
Xi, K.L., Cao, Y.C., Liu, K.Y., et al., 2019. Authigenic minerals related to wettability and their impacts on oil accumulation in tight sandstone reservoirs: an example from the Lower Cretaceous Quantou Formation in the southern Songliao Basin, China. J. Asian Earth Sci. 178, 173–192. https://doi.org/10.1016/j.jseaes.2018.04.025.
Xia, D., Li, Q., Xue, Q.Z., et al., 2016. Super flexibility and stability of graphene nanoribbons under severe twist. Phys. Chem. Chem. Phys. 18, 18406–18413. https://doi.org/10.1039/c6cp02580c.
Xiong, Y., Zhang, L., Yong, D., 1965. Analytical chemistry in the national bureau of standards: dr. David H. Freeman. Nature 208, 1259–1260. https://doi.org/10.1038/2081259c0.
Xue, Q.Z., Tao, Y.H., Liu, Z.L., et al., 2015. Mechanism of oil molecules transportation in nano-sized shale channel: MD simulation. RSC Adv. 5, 25684–25692. https://doi.org/10.1039/C4RA16682E.
Yassin, M.R., Begum, M., Dehghanpour, H., 2017. Organic shale wettability and its relationship to other petrophysical properties: a Duvernay case study. Int. J. Coal Geol. 169, 74–91. https://doi.org/10.1016/j.coal.2016.11.015.
Yekeen, N., Padmanabhan, E., Abdulelah, H., et al., 2021. CO_2/brine interfacial tension and rock wettability at reservoir conditions: a critical review of previous studies and case study of black shale from Malaysian formation. J. Petrol. Sci. Eng. 196, 107673. https://doi.org/10.1016/j.petrol.2020.107673.
Yi, H., Jia, F.F., Zhao, Y.L., et al., 2018. Surface wettability of montmorillonite (001) surface as affected by surface charge and exchangeable cations: a molecular dynamic study. Appl. Surf. Sci. 459, 148–154. https://doi.org/10.1016/j.apsusc.2018.07.216.
Yi, H., Zhang, X., Zhao, Y., et al., 2016. Molecular dynamics simulations of hydration shell on montmorillonite (001) in water. Surf. Interface Anal. 48, 976–980.

https://doi.org/10.1002/sia.6000.
Yin, X.H., Gupta, V., Du, H., et al., 2012. Surface charge and wetting characteristics of layered silicate minerals. Adv. Colloid Interface Sci. 179–182, 43–50. https://doi.org/10.1016/j.cis.2012.06.004.
Yoshimitsu, Z., Nakajima, A., Watanable, T., et al., 2002. Effects of surface structure on the hydrophobicity and sliding behavior of water droplets. Langmuir 18, 5818–5822. https://doi.org/10.1021/la020088p.
Yuan, M.Y., Nie, W., Yu, H., et al., 2021. Experimental and molecular dynamics simulation study of the effect of different surfactants on the wettability of low-rank coal. J. Environ. Chem. Eng. 3, 105986. https://doi.org/10.1016/j.jece.2021.105986.
Zhang, L.H., Lu, X.C., Liu, X.D., et al., 2016. Surface wettability of basal surfaces of clay minerals: insights from molecular dynamics simulation. Energy Fuel. 30, 149–160. https://doi.org/10.1021/acs.energyfuels.5b02142.
Zhang, W.T., Ning, Z.F., Gai, S.H., et al., 2022. Fast and effective observations of the pore structure of tight sandstones at the same location by utilizing AFM and CF-SEM. J. Petrol. Sci. Eng. 208, 109554. https://doi.org/10.1016/j.petrol.2021.109554.
Zhang, X.L., Zhao, Y.L., Zhang, Z.H., et al., 2021. Investigation of the interaction between xanthate and kaolinite based on experiments, molecular dynamics simulation, and density functional theory. J. Mol. Liq. 336, 116298. https://doi.org/10.1016/j.molliq.2021.116298.
Zhang, X.Z., Ge, J.C., Fatemeh, K., et al., 2020. Wettability of sandstone rocks and their mineral components during CO2 injection in aquifers: implications for fines migration. J. Nat. Gas Sci. Eng. 103050. https://doi.org/10.1016/j.jngse.2019.103050.
Zhao, Y., Yi, H., Jia, F., et al., 2017. A novel method for determining the thickness of hydration shells on nanosheets: a case of montmorillonite in water. Powder Technol. 306, 74–79. https://doi.org/10.1016/j.powtec.2016.10.045.
Zheng, Y., Zaoui, A., 2017. Wetting and nanodroplet contact angle of the clay 2:1 surface: the case of Na-montmorillonite (001). Appl. Surf. Sci. 396, 717–722. https://doi.org/10.1016/j.apsusc.2016.11.015.
Zhong, J., Wang, P., Zhang, Y., et al., 2013. Adsorption mechanism of oil components on water-wet mineral surface: a molecular dynamics simulation study. Energy 59, 295–300. https://doi.org/10.1016/j.energy.2013.07.016.
Zhou, G.Z., Gu, Z.B., Hu, Z.M., et al., 2020. Characterization and interpretation of organic matter, clay minerals, and gas shale rocks with low-field NMR. J. Petrol. Sci. Eng. 195, 107926. https://doi.org/10.1016/j.petrol.2020.107926.
Zhu, L., Xue, Q.Z., Li, X.F., et al., 2015. Theoretical prediction of hydrogen separation performance of two-dimensional carbon network of fused pentagon. ACS Appl. Mater. Interfaces 7, 28502–28507. https://doi.org/10.1021/acsami.5b09648.
Zou, C.N., Yang, Z., Li, W., et al., 2012. Nano oil and gas and source reservoir symbiotic oil and gas accumulation. Petrol. Explor. Dev. 39, 13–26.
Zou, C.N., Zhu, R.K., Chen, Z.Q., et al., 2019. Organic-matter-rich shales of China. Earth Sci. Rev. 189, 51–78. https://doi.org/10.1016/j.earscirev.2018.12.002.